Molecular Therapy
Original Article

miR-1293, a Candidate for miRNA-Based Cancer Therapeutics, Simultaneously Targets *BRD4* and the DNA Repair Pathway

Yuki Takagawa,[1,2] Yasuyuki Gen,[1] Tomoki Muramatsu,[1] Kousuke Tanimoto,[3] Jun Inoue,[1] Hiroyuki Harada,[2] and Johji Inazawa[1,4]

[1]Department of Molecular Cytogenetics, Medical Research Institute, Tokyo Medical and Dental University, Tokyo, Japan; [2]Department of Oral and Maxillofacial Surgery, Graduate School, Tokyo Medical and Dental University, Tokyo, Japan; [3]Genome Laboratory, Medical Research Institute, TMDU, Tokyo, Japan; [4]Bioresource Research Center, Tokyo Medical and Dental University, Bunkyo-ku, Tokyo, Japan

BRD4, a member of the bromodomain and extra-terminal domain (BET) protein family, plays a role in the organization of super-enhancers and transcriptional activation of oncogenes in cancer and is recognized as a promising target for cancer therapy. microRNAs (miRNAs), endogenous small noncoding RNAs, cause mRNA degradation or inhibit protein translation of their target genes by binding to complementary sequences. miRNA mimics simultaneously targeting several tumor-promoting genes and *BRD4* may be useful as therapeutic agents of tumor-suppressive miRNAs (TS-miRs) for cancer therapy. To investigate TS-miRs for the development of miRNA-based cancer therapeutics, we performed function-based screening in 10 cancer cell lines with a library containing 2,565 human miRNA mimics. Consequently, *miR-1293*, *miR-876-3p*, and *miR-6571-5p* were identified as TS-miRs targeting *BRD4* in this screening. Notably, *miR-1293* also suppressed DNA repair pathways by directly suppressing the DNA repair genes *APEX1* (apurinic-apyrimidinic endonuclease 1), *RPA1* (replication protein A1), and *POLD4* (DNA polymerase delta 4, accessory subunit) . Concurrent suppression of *BRD4* and these DNA repair genes synergistically inhibited tumor cell growth *in vitro*. Furthermore, administration of *miR-1293* suppressed *in vivo* tumor growth in a xenograft mouse model. These results suggest that *miR-1293* is a candidate for the development of miRNA-based cancer therapeutics.

INTRODUCTION

BRD4, a member of the bromodomain and extra-terminal domain (BET) protein family, facilitates transcriptional activation as an epigenetic reader through two bromodomains.[1] BRD4 is widely acknowledged in cancer for its role in the organization of super-enhancers and transcriptional regulation of oncogenes.[2] Pharmacological inhibition of BRD4 by BET inhibitors (BETi) has shown potent efficacy in preclinical studies against many types of cancers, such as acute myeloid leukemia,[3] multiple myeloma,[4] triple negative breast cancer,[5] melanoma,[6] pancreatic cancer,[7] and prostate cancer.[8] For this reason, BETi or the recently developed proteolysis targeting chimera (PROTAC) that degrades BRD4 is considered one of the most promising agents for the treatment of cancers.[9–11] However, a first-in-class BETi, birabresib (OTX015), has shown little but not sufficient therapeutic benefit in advanced solid tumors for use as a single agent in a clinical trial.[12] Recent studies have shown that the combination of BETi with several pathway inhibitors clearly enhanced antitumor activity in preclinical models.[10,11]

microRNAs (miRNAs), endogenous small noncoding RNAs of 20–25 nucleotides, mediate posttranscriptional gene silencing by binding to complementary mRNA sequences of their target genes.[13] Because a single miRNA can simultaneously regulate numerous target genes, miRNA mimics targeting several tumor-promoting genes may be useful as therapeutic agents for cancer therapy. From this viewpoint, we have previously identified several tumor-suppressive miRNAs (TS-miRs), including *miR-3140*, using miRNA libraries containing up to 1,090 miRNAs.[14] We showed that *miR-3140* inhibited tumor growth by concurrently targeting *BRD4* and the cell proliferation pathway (*EGFR* and *CDK2*). Nucleic acid therapeutics, including miRNA formulations, are now regarded as a next-generation treatment for cancer.[15,16]

Here, to identify candidates for the development of miRNA-based cancer therapeutics, we conducted miRNA screening using a miRNA library containing 2,565 miRNAs based on the inhibitory effects of *in vitro* tumor cell growth. We identified *miR-1293* as a TS-miR targeting *BRD4*. We further determined that the tumor-suppressive function of *miR-1293* was mediated by the combination of downregulation of BRD4 and genes associated with the DNA repair pathway. The therapeutic effects of *miR-1293* administration were evaluated using a xenograft mouse model.

Received 20 November 2019; accepted 2 April 2020;
https://doi.org/10.1016/j.ymthe.2020.04.001.

Correspondence: Yasuyuki Gen, Department of Molecular Cytogenetics, Medical Research Institute, Tokyo Medical and Dental University, Tokyo, Japan.
E-mail: ygen.cgen@mri.tmd.ac.jp
Correspondence: Johji Inazawa, Department of Molecular Cytogenetics, Medical Research Institute, Tokyo Medical and Dental University, Tokyo, Japan.
E-mail: johinaz.cgen@mri.tmd.ac.jp

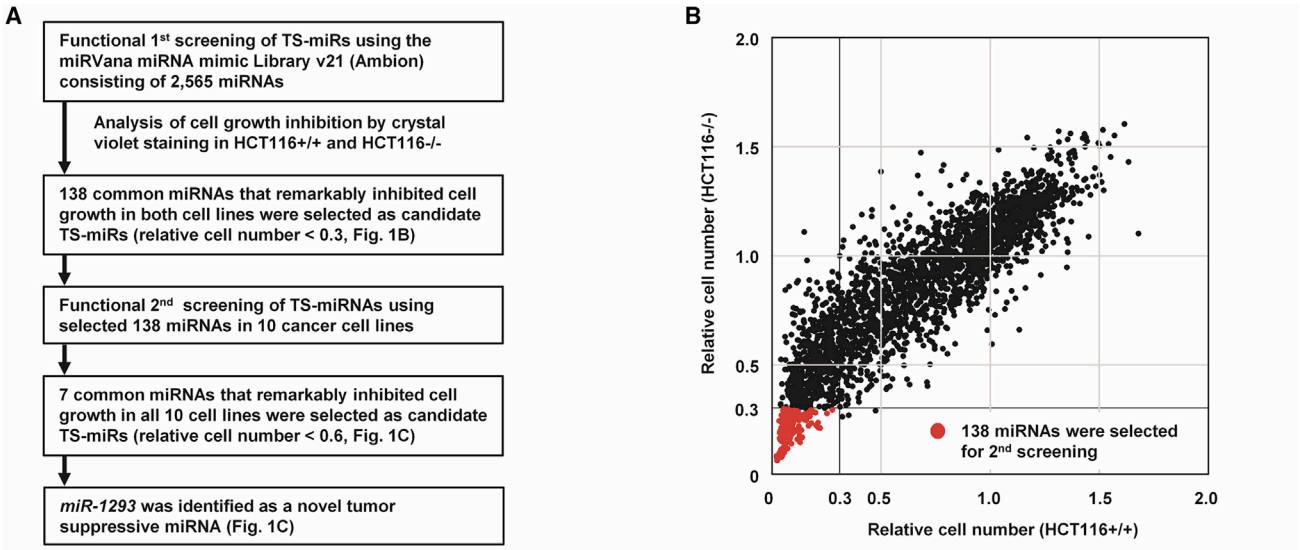

C

miRNA	Relative cell number†										Average	Location	Host gene	Ref‡
	HCT116+/+	HCT116 -/-	SW48	HT29	HOC313	HSC-2	AGS	A549	KYSE150	MIAPACA2				
hsa-miR-1293	0.15	0.13	0.29	0.36	0.44	0.36	0.17	0.16	0.22	0.08	0.24	12q13.12	*LIMA1*	-
hsamiR-876-3p	0.11	0.13	0.35	0.33	0.55	0.18	0.24	0.34	0.13	0.1	0.25	9p21.1	*LINGO2*	18
hsa-miR-4438	0.11	0.1	0.09	0.46	0.27	0.34	0.12	0.35	0.33	0.38	0.26	2q34	*SPAG16*	-
hsa-miR-6751-5p	0.05	0.09	0.25	0.43	0.59	0.34	0.48	0.25	0.16	0.19	0.28	11q13.1	*SYVN1*	-
hsa-miR-634	0.19	0.27	0.32	0.34	0.32	0.31	0.35	0.44	0.13	0.51	0.32	17q24.2	*PRKCA*	19
hsa-miR-3140-3p	0.27	0.15	0.12	0.35	0.58	0.51	0.26	0.35	0.29	0.39	0.33	4q31.3	*FBXW7*	14
hsa-miR-92a-2-5p	0.15	0.15	0.59	0.4	0.41	0.3	0.58	0.51	0.24	0.2	0.35	Xq26.2	-	-

†Relative cell number was assessed by crystal violet staining 72 hours after transfection with each miRNAs, relative to the control transfectants.
‡Reference as a tumor suppressive miRNA.

Figure 1. *miR-1293* Was Identified as a Tumor-Suppressive miRNA (TS-miR) by Function-Based miRNA Library Screening

(A) Flow chart of the study to identify TS-miRNAs. (B) Results of function-based miRNA library 1st screening in HCT116$^{+/+}$ (p53 WT) cells and HCT116$^{-/-}$ (p53 null) cells, using the mirVana miR mimic Library v21 consisting of 2,565 mature human miRNA mimics. Relative cell viability was evaluated by CV staining using a relative ratio normalized to the cell survival rate of cells transfected with negative control miRNA (*miR-NC*). Common 138 miRNAs that suppressed cell proliferation in both cell lines (red dots). (C) 7 common miRNAs that remarkably inhibited cell growth in all 10 cancer cell lines in the second screening. HCT116$^{+/+}$, SW48, AGS, and A549 cells harbor WT p53, whereas the others do not.

RESULTS

miR-1293 Was Identified as a TS-miR by a Function-Based miRNA Library Screening

To identify TS-miRs, we performed function-based miRNA screening using a library containing 2,565 miRNA mimics in HCT116 p53$^{+/+}$ (HCT116$^{+/+}$) and HCT116 p53$^{-/-}$ (HCT116$^{-/-}$) cells. A flow chart of the strategy and summary of the results are shown in Figure 1A. 72 h after transfection of each miRNA in this library, the relative cell number was assessed using a relative ratio normalized to the number of cells transfected with negative control miRNA (*miR-NC*). Figure 1B shows the results of the 1st screening in HCT116$^{+/+}$ and HCT116$^{-/-}$ cells. A total of 630 miRNAs and 141 miRNAs markedly suppressed cell proliferation (relative cell number < 0.3) in HCT116$^{+/+}$ and HCT116$^{-/-}$ cells, respectively. Since p53-inactivated cells were more resistant to cytotoxic agents than p53 wild-type (WT) cells (Figure S1), as previously reported,[17] we extracted the 138 common miRNAs that suppressed cell proliferation in both cell lines regardless of the p53 status (Table S1). We then performed a 2nd screening using these common 138 miRNAs in 10 cancer cell lines (HCT116$^{+/+}$, HCT116$^{-/-}$ [colon cancer], SW48 [colon cancer], HT29 [colon cancer], HOC313 [oral cancer], HSC-2 [oral cancer], AGS [gastric cancer], A549 [lung cancer], KYSE150 [esophageal cancer], and MIAPaCa2 [pancreatic cancer]). As shown in Figure 1C and 7 miRNAs, *miR-1293*, *miR-876-3p*, *miR-4438*, *miR-6751-5p*, *miR-634*, *miR-3140-3p*, and *miR-92a-2-5p* suppressed cell proliferation in all 10 cancer cells (relative cell number < 0.6). Among them, *miR-876-3p*, *miR-634*, and *miR-3140-3p* were previously reported as TS-miRs by our group and others.[14,18,19] Overall, *miR-1293*, *miR-4438*, *miR-6751-5p*, and *miR-92a-2-5p* were identified as TS-miRs.

miR-1293 Suppressed the Expression of BRD4 by Directly Targeting Its 3′ UTR

We have previously shown that *miR-3140-3p*, one of 7 TS-miRs identified in this screening, exerts tumor-suppressive effects by targeting

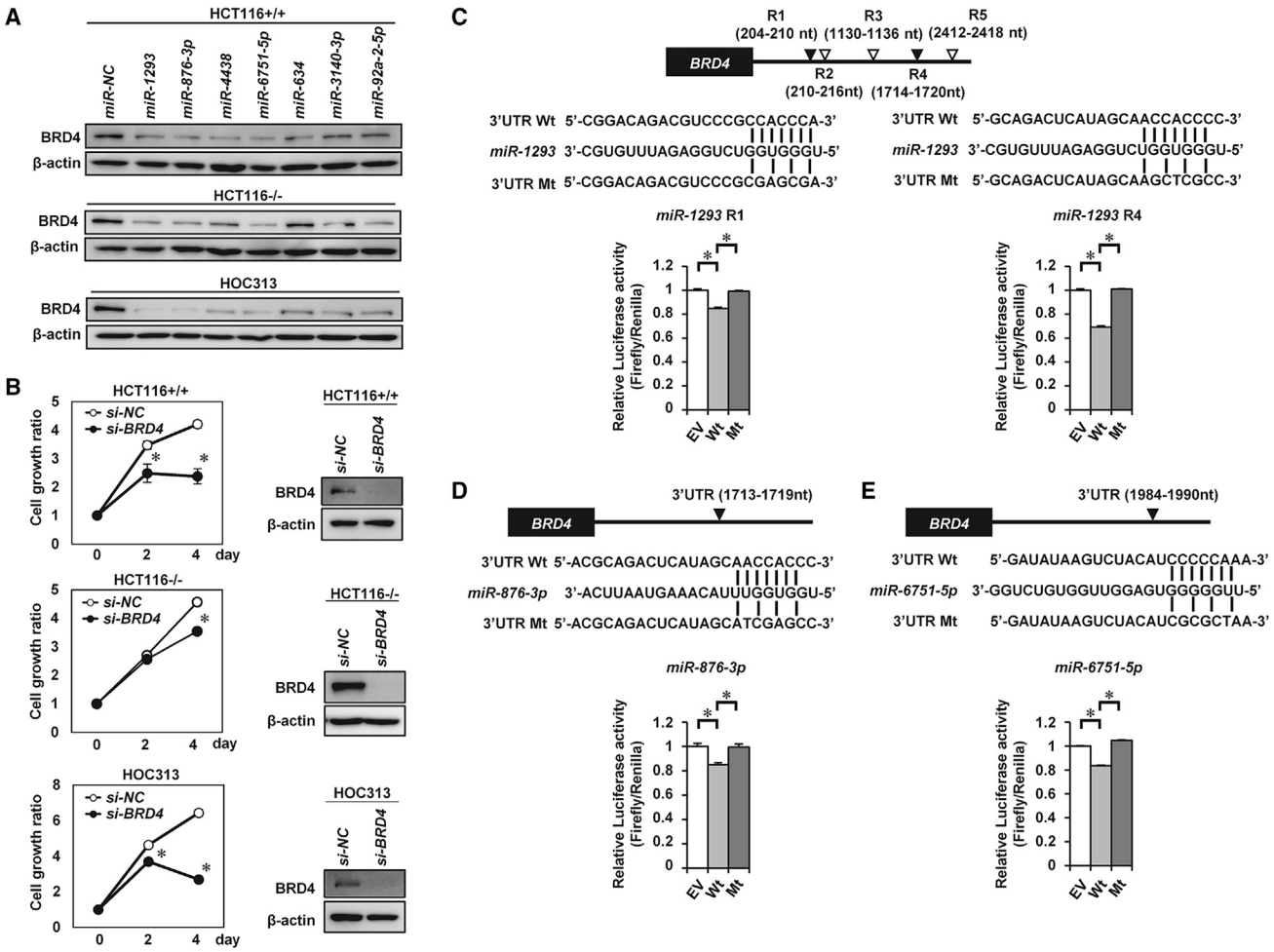

Figure 2. *miR-1293* Directly Targets the 3′ UTR of *BRD4*

(A) Western blot analysis of BRD4 in HCT116$^{+/+}$, HCT116$^{-/-}$, and HOC313 cells 48 h after transfection with 10 nmol/L *miR-NC* or the indicated 7 miRNAs. (B) Knocking down *BRD4* suppressed *in vitro* cell proliferation in HCT116$^{+/+}$, HCT116$^{-/-}$, and HOC313 cells. Western blot analysis (right) and cell growth assay (left) in each cell line after transfection with 20 nmol/L negative control siRNA (*si-NC*) or siRNA targeting *BRD4* (*si-BRD4*). *p < 0.05. (C–E) Luciferase reporter assay. HOC313 cells were cotransfected with pmirGLO dual-luciferase vectors containing wild-type (WT) *BRD4*-3′ UTR or mutant variants of *BRD4*-3′ UTR and *miR-NC*, *miR-1293* (C), *miR-876-3p* (D), or *miR-6751-5p* (E). Top, putative binding sequences of each miRNA within the 3′ UTR of *BRD4* and mutant sequences are indicated. Bottom, the results of the luciferase assay; *p < 0.05.

BRD4, *EGFR*, and *CDK2* simultaneously.[14] A recent study revealed that targeting *BRD4* and other pathway inhibitors has synergistic antitumor activity.[11,20,21] Thus, we explored TS-miRs directly targeting *BRD4*. First, we determined whether those 7 TS-miRs downregulate the expression of BRD4 in all 10 cell lines. As shown in Figures 2A and S2A, the expression of BRD4 was decreased in all 10 cell lines transfected with *miR-1293*, *miR-876-3p*, *miR-6751-5p*, *miR-3140-3p*, and *miR-92a-2-5p*, although the expression of BRD4 was not decreased in HCT116$^{-/-}$, MIAPaCa2, and AGS cells transfected with *miR-634*, and in HT29 and AGS cells transfected with *miR-4438*. Knockdown of *BRD4* using small interfering RNA (siRNA) targeting *BRD4* (*si-BRD4*) reduced cell proliferation in all 10 cell lines (Figure 2B; Figures S2B and S2C), suggesting that downregulation of BRD4 is one of the tumor-suppressive mechanisms of these TS-miRs except for *miR-634* and *miR-4438*.

We next examined whether each of the 7 miRNAs could directly bind to the 3′ UTR of *BRD4*. Five miRNAs except for *miR-634* and *miR-3140-3p* were predicted to bind to the 3′ UTR of *BRD4* according to the TargetScan program (http://www.targetscan.org). Luciferase assays, using reporter plasmid vectors containing WT or mutant (Mt) seed sequences of the 3′ UTR of *BRD4* mRNA were performed in HOC313 cells (Figures 2C–2E; Figures S3A–S3C). The luciferase activity of the WT vector was decreased compared with that of the empty vector (EV) in *miR-1293*-, *miR-876-3p*-, and *miR-6751-5p*-transfected cells and was completely restored with the Mt vector, suggesting that *miR-1293*, *miR-876-3p*, and *miR-6751-5p* can directly bind to the 3′ UTR of *BRD4*. On the other hand, *miR-4438* and *miR-92a-2-5p* could not bind the 3′ UTR or coding sequence (CDS) of *BRD4* (Figures S3B and S3C). Collectively, these data suggested that *miR-1293*, *miR-876-3p*, and *miR-6751-5p* are TS-miRs targeting *BRD4*.

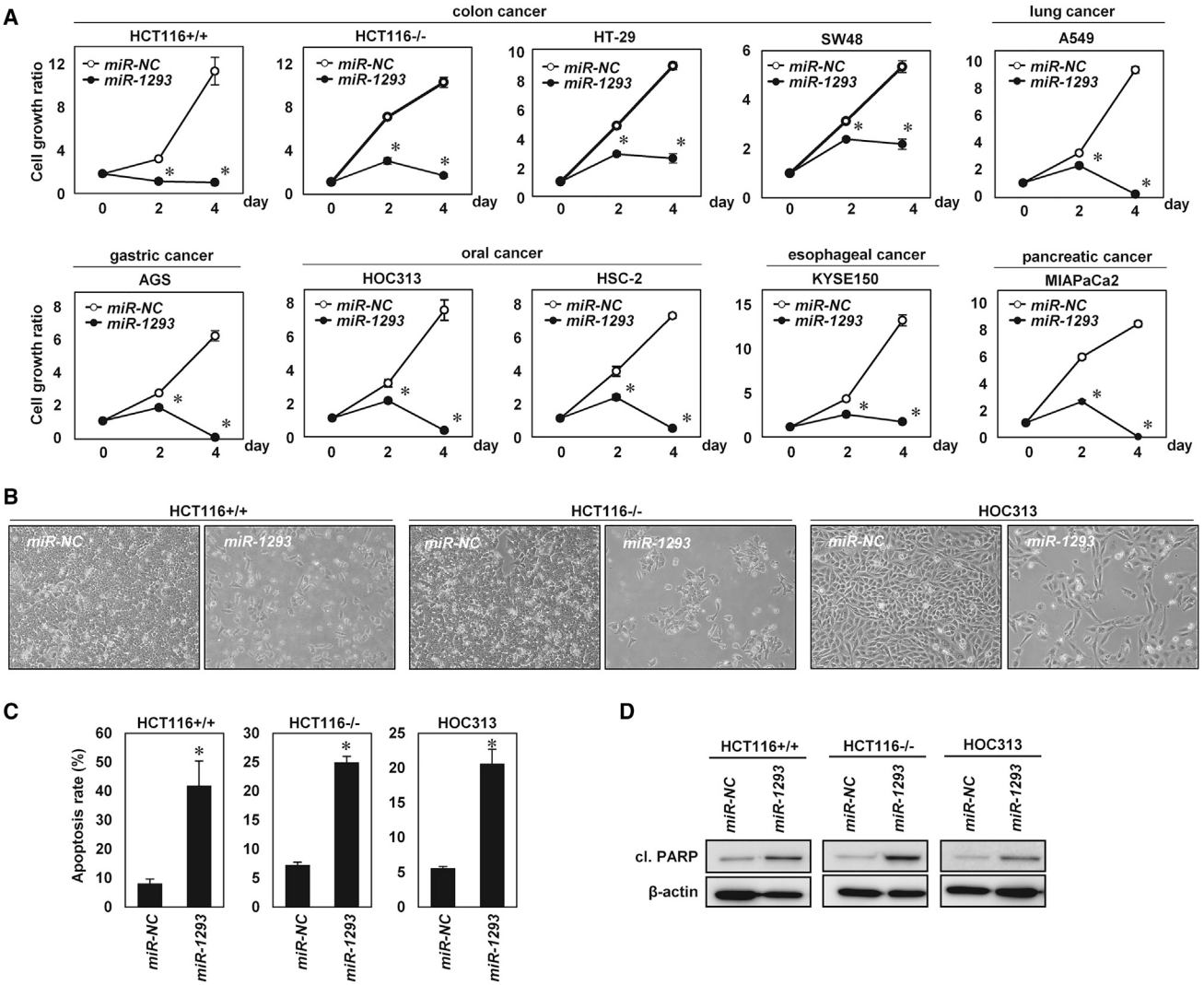

Figure 3. Overexpression of *miR-1293* Induced Apoptosis in Cancer Cells *In Vitro*

(A) *In vitro* cell growth assay in various cancer cell types. Cells were transfected with 10 nmol/L *miR-NC* or *miR-1293*. Cell growth rate was assessed with the CV staining assay using a relative ratio compared with cell growth on day 0. Error bar, SD for triplicate experiments. *$p < 0.05$. (B) Phase contrast images of HCT116$^{+/+}$, HCT116$^{-/-}$, and HOC313 cells transfected with 10 nmol/L *miR-NC* or *miR-1293*. Images were obtained 48 h after transfection. (C) The percentage of apoptotic cells in HCT116$^{+/+}$, HCT116$^{-/-}$, and HOC313 cells transfected with *miR-NC* or *miR-1293*. Cells were double stained with Annexin V and propidium iodide (PI) 48 h after transfection and analyzed by flow cytometry. The percentage of cells indicates late apoptotic cells (Annexin V+/ PI+). Error bar, SD for triplicate experiments. *$p < 0.05$. (D) Western blot analysis of cleaved PARP (cl. PARP) in HCT116$^{+/+}$, HCT116$^{-/-}$, and HOC313 cells 48 h after transfection with 10 nmol/L *miR-NC* or *miR-1293*.

miR-1293 Inhibited *In Vitro* Tumor Cell Growth in Various Cancer Cell Lines

We next focused on a detailed analysis of *miR-1293* because *miR-1293* is a TS-miR that inhibited *in vitro* tumor cell growth most efficiently in the 2nd screening. To validate the growth-suppressive effect of *miR-1293*, we evaluated cell proliferation *in vitro* after transfections of various cell lines with *miR-1293* or *miR-NC*. In agreement with the results of the 2nd screening, overexpression of *miR-1293* significantly inhibited tumor cell proliferation in these cell lines (Figures 3A and 3B; Figure S4A). Annexin V and propidium iodide (PI) staining showed that the apoptotic cell population was increased in *miR-1293*-transfected cells compared with *miR-NC*-transfected cells (Figure 3C; Figure S4B). Western blotting showed increased expression of cleaved PARP (cl. PARP) in *miR-1293*-transfected cells (Figure 3D; Figure S4C). Taken together, the results demonstrate that *miR-1293* inhibited *in vitro* tumor cell growth by inducing apoptosis.

miR-1293 Directly Targeted *APEX1*, *RPA1*, and *POLD4* by Binding Their 3′ UTRs

To explore target genes of *miR-1293* other than *BRD4*, we performed gene expression array analysis in 5 cell lines, HCT116$^{+/+}$, A549, KYSE150, HOC313, and HSC-2, after transfection of *miR-1293* or

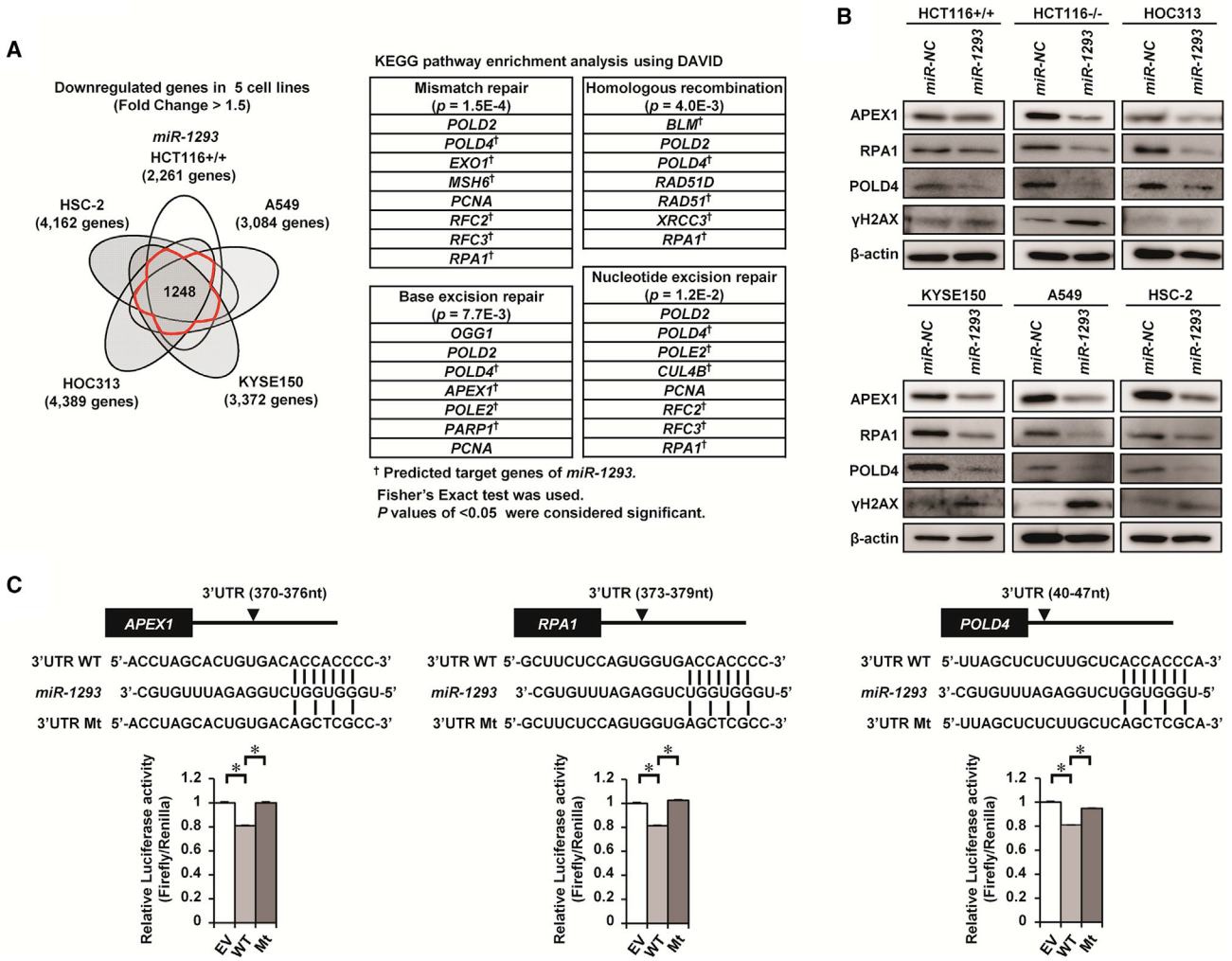

Figure 4. *miR-1293* Downregulated the Expression of *APEX1*, *RPA1*, and *POLD4* by Directly Targeting Their 3′ UTRs

(A) Identification of downregulated genes and pathways after *miR-1293* transfection. Left, a Venn diagram showing 1,248 genes that were commonly downregulated (fold change > 1.5) by transfection of *miR-1293* in at least 4 out of 5 cell lines. Right, the table shows the results of the pathway analysis of the 1,248 commonly downregulated genes using DAVID Bioinformatics Resources 6.8. Fisher's exact test was used for genes selection. $p < 0.05$ were considered significant. (B) Western blot analysis of APEX1, RPA1, POLD4, and γH2AX in HCT116$^{+/+}$, HCT116$^{-/-}$, HOC313, KYSE150, A549, and HSC-2 cells 48 h after transfection with 10 nmol/L *miR-NC* or *miR-1293*. (C) Luciferase reporter assays. HOC313 cells were cotransfected with pmirGLO dual-luciferase vectors containing the wild-type (WT) 3′ UTRs of *APEX1*, *RPA1*, and *POLD4* or mutant (Mt) variants of these genes and *miR-NC* or *miR-1293*. Top, putative binding site of *miR-1293* within the 3′ UTR of each gene and mutant sequences. Bottom, the results of the luciferase assay; *$p < 0.05$.

miR-NC. As shown in a Venn diagram (Figure 4A), 1,248 genes were commonly downregulated (fold change > 1.5) by transfection of *miR-1293* in 4 or 5 out of 5 cell lines. The Kyoto Encyclopedia of Genes and Genomes (KEGG) pathway enrichment analysis of these 1248 genes using DAVID Bioinformatics Resources 6.8 (https://david.ncifcrf.gov/) revealed that *miR-1293* significantly suppressed several genes related to DNA repair pathways, such as base excision repair, nucleotide excision repair, mismatch repair, and homologous recombination (HR) (Figure 4A; Figure S5A). We then examined whether genes associated with the DNA repair pathway might be direct targets of *miR-1293*. Among these targets, *APEX1* (apurinic-apyrimidinic endonuclease 1), *RPA1* (replication protein A1), and *POLD4* (DNA polymerase delta 4, accessory subunit) were decreased at protein levels in *miR-1293*-transfected HCT116$^{+/+}$, HCT116$^{-/-}$, HOC313, KYSE150, A549, and HSC-2 cells compared with those in *miR-NC*-transfectants (Figure 4B; Figure S6A). The expression of γH2AX, a marker of DNA damage, was also increased in *miR-1293*-transfected cells, especially in HCT116$^{-/-}$ and A549 cells (Figure 4B; Figure S6B). Luciferase assays using reporter plasmid vectors with WT or Mt seed sequences of the 3′ UTRs of *APEX1*, *RPA1*, and *POLD4* showed that in *miR-1293*-transfected cells, the luciferase activity was significantly decreased in the WT vector compared with the EV, whereas it was completely restored in the Mt vector (Figure 4C). The luciferase activity of the WT vector containing the predicted seed sequences in the 3′

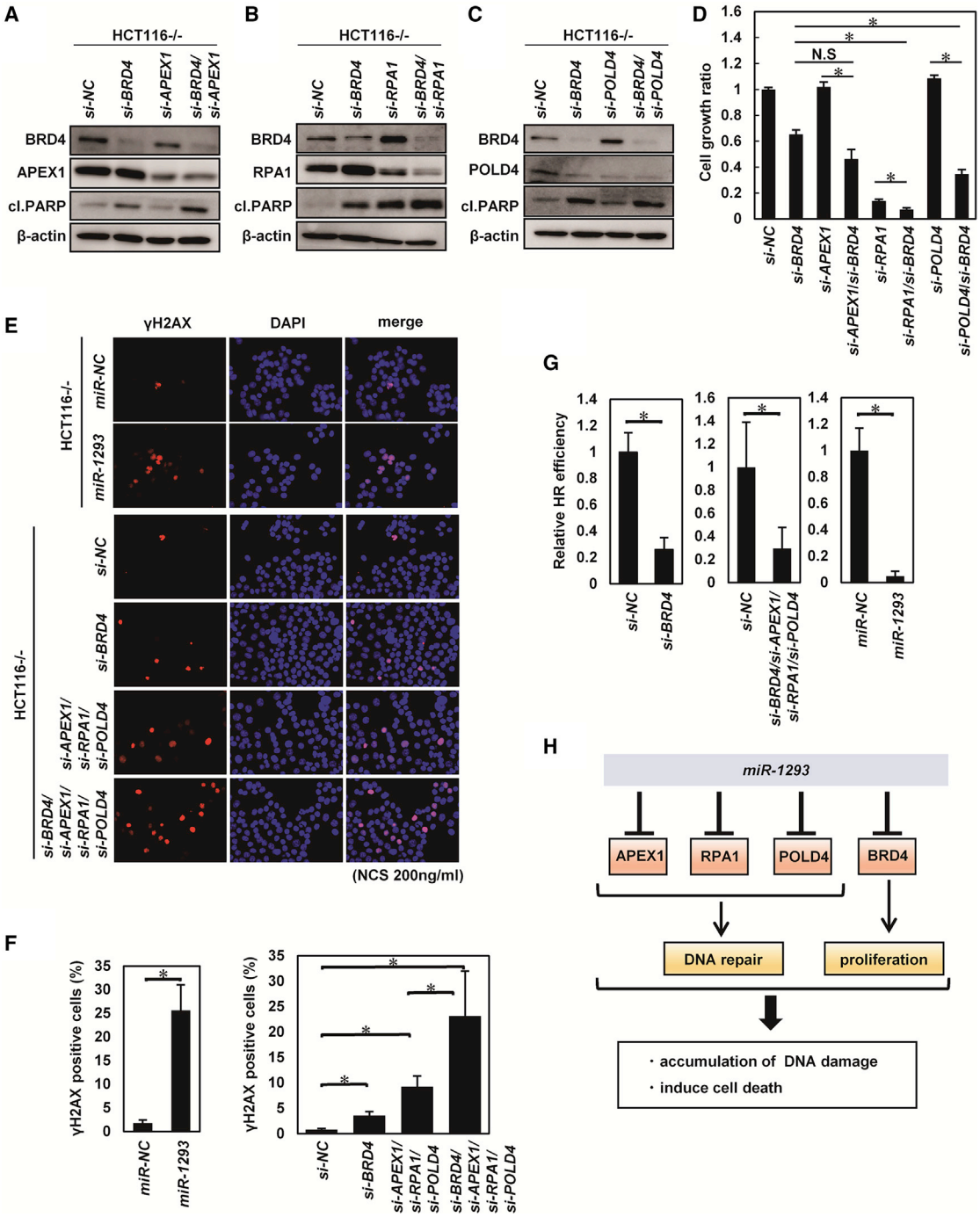

Figure 5. *miR-1293* Inhibited DNA Damage Repair by Downregulating BRD4 and DNA Repair Genes Synergistically *In Vitro*

(A–D) Evaluation of the effect of *si-BRD4* and *si-APEX1*, *si-RPA1*, or *si-POLD4*. Western blot analysis (A, *si-BRD4* and *si-APEX1*; B, *si-BRD4* and *si-RPA1*; C, *si-BRD4* and *si-POLD4*) and cell growth assay (D) in indicated cell lines after transfection with siRNA (*si-NC* [40 nmol/L]; *si-BRD4*, *si-APEX1*, *si-RPA1*, and *si-POLD4* [each 20 nmol/L]). 120 h after transfection with the siRNAs, the cell growth rate was assessed with the CV staining assay using a relative ratio compared with that of *si-NC*-transfected cells. Error bar, SD for triplicate experiments. *$p < 0.05$. (E) Immunofluorescence analysis of HCT116$^{-/-}$ cells that were double labeled with anti-γH2AX (red) and DAPI (blue; nuclei). Cells were transfected with 10 nmol/L *miR-NC*, *miR-1293*, *si-NC*, or the indicated siRNAs for 6 h following treatment with neocarzinostatin (200 ng/mL) for 30 min. (F) The

(legend continued on next page)

UTR or CDS of *RAD51*, *XRCC3*, *BLM*, *POLE2*, *PARP1*, *EXO1*, or *MSH6* was not decreased in *miR-1293*-transfectants (Figure S5B). The protein levels of *CUL4B*, *RFC2*, and *RFC3*, which were also listed in the present KEGG pathway enrichment analysis, were not reduced appreciably in *miR-1293*-transfected cells (Figure S5C). Overall, *miR-1293* directly suppressed the expression of *APEX1*, *RPA1*, and *POLD4* by binding the 3′ UTRs of these genes.

miR-1293 Suppressed *In Vitro* Tumor Cell Growth by Concurrent Downregulation of *BRD4*, *APEX1*, *RPA1*, and *POLD4*

We next examined the effects of concurrent downregulation of *BRD4*, *APEX1*, *RPA1*, and *POLD4* using siRNA targeting each gene. As shown in Figures 5A–5D, knockdown of *BRD4* in combination with knockdown of *RPA1* or *POLD4* led to a more pronounced suppression of i*n vitro* cell growth with increased expression of cl. PARP in HCT116$^{-/-}$ cells, although these synergistic effects of combination of *si-BRD4* and *si-APEX1* were not significant. Similar synergistic effects on cell growth were also observed in HOC313 cells, although those were not significant in HCT116$^{+/+}$ cells (Figure S7A). Collectively, these results suggested that concurrent downregulation of *BRD4*, *RPA1*, and *POLD4* may contribute to the *miR-1293*-mediated growth-suppressive effects.

Next, to examine the effects of *miR-1293* on DNA repair, the accumulation and clearance of DNA damage were evaluated in *miR-1293*- and *miR-NC*-transfected HCT116$^{-/-}$ and HOC313 cells following neocarzinostatin (NCS) treatment. We observed a significantly delayed clearance of γH2AX foci, a marker of unrepaired DNA damage, in *miR-1293*-transfected cells compared *miR-NC*-transfected cells (Figures 5E and 5F; Figure S7B). These results were partially reproduced by the combined knockdown of *APEX1*, *RPA1*, *POLD4*, and *BRD4*. We also evaluated the frequency of HR, a major pathway of double-stranded DNA break repair, using the DR-GFP reporter in U2OS cells as previously reported.[22] The HR efficiency of U2OS DR-GFP cells transfected with *miR-1293* was significantly decreased (Figure 5G). Knockdown of *BRD4*, *APEX1*, *RPA1*, and *POLD4* also suppressed the HR efficiency in HCT116$^{-/-}$ cells. Collectively, these results demonstrated that *miR-1293* inhibited tumor cell growth and the DNA repair pathway by concomitant suppression of *BRD4*, *APEX1*, *RPA1*, and *POLD4* (Figure 5H).

miR-1293 Suppressed *In Vivo* Tumor Growth in a Xenograft Mouse Model

The *in vivo* therapeutic effect of *miR-1293* was investigated using a xenograft mouse model of HCT116$^{-/-}$ cells. *miR-NC* or *miR-1293* was administered into the subcutaneous space around tumors 5 times (3, 7, 10, 14, and 17 days after the injection of cells; Figure 6A). There were no obvious adverse consequences, such as body weight loss or skin damage around the administration site of miRNAs (Figure S8A). As a result, tumors treated with *miR-1293* at 19 days after the injection of HCT116$^{-/-}$ cells were significantly smaller than tumors treated with *miR-NC* (Figures 6B–6D). qRT-PCR and *in situ* hybridization showed that the expression of *miR-1293* was significantly higher in the *miR-1293*-treated tumors compared to the *miR-NC*-treated tumors, suggesting that *miR-1293* was actually delivered into the cancer cells of the *miR-1293*-treated tumor (Figure 6E; Figure S8B). Immunohistochemical staining showed that the expression levels of BRD4, APEX1, RPA1, and POLD4 were decreased in the resected tumors treated with *miR-1293* (Figure 6F). Similarly, administration of *miR-1293* inhibited tumor growth in nude mice that were subcutaneously inoculated with SAS cells, as well as *in vitro* (Figures S8C–S8H and S9A–S9M). Taken together, these findings suggest that the administration of *miR-1293* might be effective for tumor growth suppression *in vivo*.

DISCUSSION

Here, we identified *miR-1293*, *miR-876-3p*, and *miR-6751-5p* as TS-miRs targeting BRD4 by function-based screening of 2,565 miRNAs. We showed that *miR-1293* suppressed DNA repair pathways by concurrently targeting *BRD4*, *APEX1*, *RPA1*, and *POLD4*, thereby inhibiting tumor cell growth. Administration of *miR-1293* suppressed *in vivo* tumor growth in a xenograft mouse model.

Previous studies, including ours, have reported the results of function-based miRNA library screening in cancer cells. For example, we previously screened the growth-suppressive effects of 1,090 human miRNAs in pancreatic cancer cells,[14] and Zhou et al.[23] examined a total of 858 human miRNAs in *KRAS* mutant cancer cells. Since 2,654 mature human miRNAs are currently registered in miRBase v22 (http://www.mirbase.org/), the tumor-suppressive functions of numerous human miRNAs have not yet been investigated. Thus, we examined a total of 2,565 miRNAs, which covered ~96% of the registered human miRNAs, on the basis of their growth-inhibitory effects in cancer cells. In agreement with past reports including ours, the results of the 1st screening included several known TS-miRs, such as *miR-1298-3p*, *miR-491-5p*, *miR-634*, and *miR-3140-3p* (Table S1).[14,19,23,24] Furthermore, the 2nd screening identified 7 miRNAs as the most growth-inhibitory miRNAs in all 10 cancer cell lines tested.

Since BRD4 regulates the expression of genes associated with cancer cell growth, BRD4-targeting therapy such as BETi or PROTAC that degrade BRD4 was reported to exhibit potent efficacy against many types of cancer.[2–8,10] Thus, TS-miRs targeting BRD4 are a reasonable strategy for the development of miRNA-based therapeutics. Our results showed that *miR-1293*, *miR-876-3p*, and *miR-6751-5p* are TS-miRs targeting BRD4. Since recent studies have shown that the combined inhibition of BRD4 and other signaling pathways markedly enhanced antitumor activity,[10,11] these TS-miRs, similar to *miR-*

percentage of γH2AX-positive cells in (E). *p < 0.05. (G) Homologous recombination (HR) repair analysis. U2OS DR-GFP cells were transfected with *si-NC*, the indicated siRNAs, *miR-NC*, or *miR-1293*, 6 h after transfection with the I-Sce1 endonuclease expression vector for 48 h. The HR efficiency of cells cotransfected with *si-BRD4* and *miR-1293* was compared with that of cells cotransfected with *si-NC* and *miR-NC* based on the percentage of GFP+ cells detected by flow cytometry. Error bar, SD for triplicate experiments. *p < 0.05. (H) Schematic models for the mechanism by which *miR-1293* suppresses the DNA repair pathway and tumor growth.

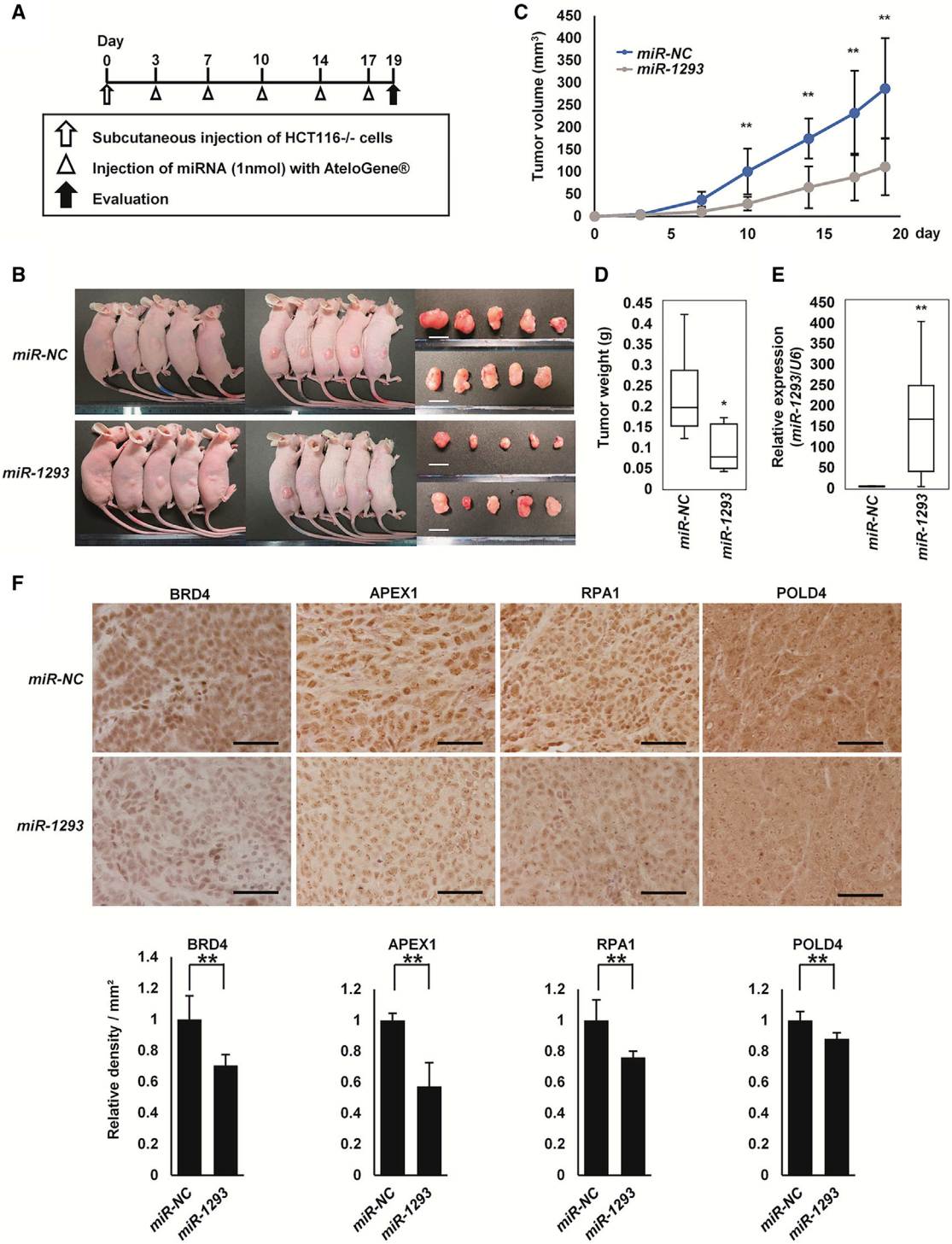

Figure 6. Therapeutic Effects of *miR-1293* on Tumor Growth *In Vivo*

(A) The experimental schedule for *miR-1293* treatment in nude mice. Tumors were formed by subcutaneous injection of HCT116$^{-/-}$ cells in nude mice. *miR-NC* or *miR-1293* was administered subcutaneously around the tumors for a total of 5 times (3, 7, 10, 14, and 17 days after the injection of cells). (B) Representative images of tumor-bearing nude mice and resected tumors at 19 days after the injection of HCT116$^{-/-}$ cells. Scale bar, 10 mm. (C) Tumor growth curves of xenograft mouse models treated with *miR-NC* or *miR-1293* (n = 10, each). Tumor volume was calculated using the following formula: (shortest diameter) ^{2} × (longest diameter) × 0.5. Error bar, SD for 10 mice; *p <

(legend continued on next page)

3140-3p,[14] may suppress BRD4 and other oncogenic targets concomitantly.

According to the TCGA database, the expression of *miR-1293*, *miR-876*, and *miR-6751* are extremely low in comparison to the expression of the representative miRNA *miR-34a* in both tumor tissues and non-tumor tissues of colon, esophagus, head and neck, lung, pancreas, and stomach, although the expression of *miR-1293* is slightly elevated in esophagus squamous cell carcinoma (ESCC) and head and neck squamous cell carcinoma (HNSCC) (Figure S10A). The expression of *miR-1293* was not correlated with overall survival in ESCC, and HNSCC (Figure S10B). On the other hand, the expression of *miR-1293* was reported to be decreased in the serum of patients with colon cancer[25] and to be increased in the tissues of oral cancer.[26] Further investigation of the clinical relevance of *miR-1293* is required.

Moreover, we showed that *miR-1293* directly suppressed the DNA repair genes *APEX1*, *RPA1*, and *POLD4*. APEX1, a key enzyme for the repair of single-strand DNA breaks, is frequently overexpressed in solid tumors.[27–29] RPA1, one of the main eukaryotic single-stranded DNA-binding proteins, plays an important role in DNA damage repair by recognizing DNA damage. Overexpression of RPA1 has been reported to be associated with poor clinical outcomes in several cancers.[30–32] POLD4 not only plays a critical role in DNA replication and repair,[33] but also promotes tumor cell growth.[34] Since cancer cells depend more on DNA repair than normal cells because of oncogene-induced replication stress,[35] targeting DNA repair genes such as *APEX1*, *RPA1*, and *POLD4* may be rational for cancer therapy.

Recent studies revealed that BRD4 promotes DNA damage repair, including the non-homologous end-joining recombination pathway and HR pathway,[20,36,37] and consequently, inhibition of the DNA repair pathway along with BRD4 suppression is synthetically lethal in many types of cancer cells.[20,36,37] Consistent with these reports, we showed that concurrent downregulation of *BRD4*, *APEX1*, *RPA1*, and *POLD4* synergistically suppressed DNA repair and inhibited tumor cell growth *in vitro*. Since these effects were similar to those of *miR-1293*, the tumor-suppressive effects of *miR-1293* are thought to be mediated by the concurrent targeting of *BRD4*, *APEX1*, *RPA1*, and *POLD4*. The combination of *miR-1293* with DNA-damaging agents or radiation therapy may be effective for cancer therapy.

Finally, we showed that local administration of *miR-1293* suppressed *in vivo* tumor growth without obvious adverse events. These results indicated the potential of *miR-1293* for miRNA-based therapy. For future studies, to translate these findings into the clinical, several challenges need to be overcome that include chemical modification of the nucleic acids for improved stability, development of a drug delivery system, and evaluation of the effects of *miR-1293* on normal cells.[15] In conclusion, *miR-1293* suppresses tumor cell growth by concurrently targeting *BRD4* and DNA repair genes. *miR-1293* may be a promising candidate for the development of miRNA-based cancer therapeutics.

MATERIALS AND METHODS

Cell Culture

The human colon cancer cell line HCT116 ($HCT116^{+/+}$) and its derived isogenic p53 null cell line ($HCT116^{-/-}$) were kindly provided by Dr. Bert Vogelstein (The Johns Hopkins University). $HCT116^{+/+}$, $HCT116^{-/-}$, HT29, SW48, MIAPaCa2, HSC2, HOC313, and A549 cells were maintained in Dulbecco's modified Eagle's medium containing 10% fetal bovine serum (FBS). KYSE150 cells, a gift from Dr. Y. Shimada (Toyama University),[38] and AGS cells were maintained in RPMI 1640 medium containing 10% FBS. SAS cells were maintained in Dulbecco's modified Eagle's medium with Ham's F12 medium containing 10% FBS. All cell lines were maintained at 37°C and 5% CO_2. All experiments were carried out in accordance with the approved guidelines and regulations (G2019-013A).

Reagents

Olaparib (AZD2281, Ku-0059436; S1060) was purchased from Selleck Chemicals (Houston, TX), puromycin was obtained from Invivogen (San Diego, CA), neocarzinostatin (N9162) was purchased from Sigma-Aldrich (St. Louis, MO), and doxorubicin hydrochloride was obtained from WAKO Pure Chemical Industries (Tokyo, Japan). These reagents were used for the treatment of cultured cells *in vitro* at the indicated concentrations.

Function-Based miRNA Screening

In the 1st screening, 6,000 $HCT116^{+/+}$ and $HCT116^{-/-}$ cells were seeded in 96-well plates. After 24 h, each cell line was transfected in duplicate with each of the 2,565 double-stranded RNAs (dsRNA) from the mirVana miR mimic Library v21 (Thermo Fisher Scientific, Waltham, MA) or a negative control miRNA (*miR-NC*) using an RNA concentration of 10 nmol/L. After 72 h, viable cell numbers were assessed by the crystal violet (CV) staining assay. The results were normalized to the numbers of cells transfected with *miR-NC*. In the 2nd screening, $HCT116^{+/+}$, $HCT116^{-/-}$ (colon cancer), SW48 (colon cancer), HT29 (colon cancer), HOC313 (oral cancer), HSC-2 (oral cancer), AGS (gastric cancer), A549 (lung cancer), KYSE150 (esophageal cancer), and MIAPaCa2 (pancreatic cancer) cells were used. 24 h after cell seeding, each cell line was transfected in duplicate with each of the 138 dsRNAs selected from the 1st screening or a *miR-NC* using an RNA concentration of 10 nmol/L. After 72 h, viable cell numbers were assessed as described above.

0.05, **p < 0.01. (D) Weights of the resected tumors. Tumor weights are shown as a boxplot. Error bar, SD for 10 mice; *p < 0.05. (E) Expression analysis of *miR-1293* in the resected tumors. The expression level of *miR-1293* was measured by qRT-PCR. Each experiment was performed in duplicate. The relative ratio was normalized to the expression of *RNU6B*. Error bar, SD for 10 mice; **p < 0.01. (F) Representative images (upper) and evaluation (lower) of immunohistochemical staining for BRD4, APEX1, RPA1, and POLD4 in resected tumors. The density per field was defined using the single point selection tool on the Nikon NIS Elements Br 4.0 software, and the results were normalized to the values of tumors treated with *miR-NC* (see the Materials and Methods section). Scale bar, 50 μm. **p < 0.01.

Transfection of miRNAs and siRNAs

The dsRNAs mimicking mature human *miR-1293* (MC13698), *miR-876-3p* (MC12886), *miR-4438* (MC22634), *miR-6751-5p* (MC27194), *miR-634* (MC11538), *miR-3140-3p* (MC17496), and *miR-92a-2-5p* (MC12524) and a nonspecific control miRNA (negative control #1) were purchased from Thermo Fisher Scientific. The SMARTpool siRNA for *BRD4* (M-004937-02), *APEX1* (M-010237-01), *RPA1* (M-015749-01), *POLD4* (M-014013-01), and nonspecific control siRNAs were obtained from GE Healthcare (Buckinghamshire, UK). Each SMARTpool siRNA contains 4 siRNA duplexes designed to target different mRNA sequences of the same gene. miRNAs and siRNAs were transfected individually into cells at the indicated concentrations using Lipofectamine RNAiMAX (Thermo Fisher Scientific) according to the manufacturer's instructions.

In Vitro Cell Growth Assay

Cell survival was evaluated by the CV staining assay. Cells were washed in PBS and fixed with 0.1% CV in 10% formaldehyde in PBS for 5 minutes. After the excess CV solution was discarded, stained cells were completely air-dried, and then lysed with a 2% SDS solution with shaking for 1 h. Optical density (OD) absorbance was measured at 560 nm using a microplate reader (ARVOmx; PerkinElmer), and the percent absorbance of every well was determined. The OD absorbance values of cells in control wells were arbitrarily set at 100% to determine the percentage of viable cells.

Apoptosis Assay

48 h after transfection with 10 nmol/L miRNA (*miR-NC* or *miR-1293*), HCT116$^{+/+}$, HCT116$^{-/-}$, and HOC313 cells were double stained with Annexin V-FITC and PI using a MEBCYTO Apoptosis kit (MBL, Nagoya), according to the manufacturer's instructions. Cells were analyzed by the Accuri C6 Flow Cytometer (BD Biosciences).

Gene Expression Array Analysis

Gene expression array analysis was carried out as previously described.[19] Briefly, HCT116$^{+/+}$, A549, KYSE150, HOC313, and HSC-2 cells were transfected with 10 nmol/L miRNA (*miR-NC* or *miR-1293*). Total RNA was extracted 48 h after transfection. For gene expression analysis, the Agilent 8 × 60 K array was used according to the manufacturer's instructions (Agilent Technologies). The data were analyzed by GeneSpring software (Agilent Technologies, Japan).

Western Blotting

Western blotting was performed as previously described.[19] The following primary antibodies were used for western blotting: antibodies against BRD4 (#13440), cleaved PARP (#9541), phospho-histone H2AX (Ser139) (#9718), and RPA70 (#2267) were purchased from Cell Signaling Technology; the antibody against APEX1 (10203-1-AP) was purchased from Proteintech (Chicago, IL); anti-POLD4 antibody (MBS9609765) was obtained from MyBioSource.com (San Diego, CA, USA); and anti-β-actin (A5441) and anti-Vinculin (V9131) were obtained from Sigma-Aldrich (Tokyo, Japan).

Luciferase Activity Assay

The luciferase activity assay was carried out as previously described.[19] Luciferase reporter plasmids were constructed by inserting the 3′ UTRs of *BRD4*, *APEX1*, *RPA1*, and *POLD4* downstream of the luciferase gene in the pmirGLO Dual-Luciferase miRNA Target Expression Vector (Promega, Madison, WI). All site-specific mutations were generated by the KOD -Plus- Mutagenesis Kit (TOYOBO, Osaka, Japan). Luciferase reporter plasmids or the control plasmid (pmirGLO) were transfected into HOC313 cells using Lipofectamine 2000 (Thermo Fisher Scientific), and 10 nmol/L of the indicated miRNA mimic was also transfected 6 h later. After 2 days, firefly and Renilla luciferase activities were measured using the Dual-Luciferase Reporter Assay System (Promega), and relative luciferase activity was calculated by normalizing the firefly luciferase reading to its corresponding internal Renilla luciferase control.

Plasmid Construction and Transfection

The BRD4 expression vector was previously generated.[14] The BRD4 expression vector was transfected into MIAPaCa2 cells using Lipofectamine 2000 (Thermo Fisher Scientific) according to the manufacturer's instructions.

Immunofluorescence Analysis

Immunofluorescence was carried out as described previously.[39] For immunostaining of phospho-histone H2AX, cells were fixed with 3.7% formaldehyde, permeabilized with 0.1% Triton X-100, blocked with 3% bovine serum albumin for 30 min, and then incubated with primary antibodies (rabbit anti-phospho-histone H2AX, 1:400 dilution) for 12 h at 4°C. Bound antibodies were visualized using Alexa Fluor 555-conjugated anti-rabbit immunoglobulin G (IgG) antibody (both 1:500 dilution; Life Technologies), and coverslips were mounted in VECTASHIELD containing DAPI (Vector). Images were obtained by confocal fluorescence microscopy (Nikon).

In Vivo Tumor Growth and miRNA Administration

In vivo miRNA administration was performed as previously described.[19] 6-week-old female BALB/c nude mice were purchased from Oriental Bio Service, Japan. Briefly, a total of 2.0 × 10^6 cells in 100 μL of PBS were subcutaneously injected into the dorsal side of the mice. After tumor formation on day 3, a mixture of 1 nmol dsRNA (*miR-NC* or *miR-1293*) and 100 μL AteloGene (KOKEN, Tokyo, Japan) was administered around the tumor. miRNAs were administered on days 3, 7, 10, 14, and 17, and, on day 19 after cell injection, mice were sacrificed and tumors were resected. Tumor volume was calculated using the following formula: $(\text{shortest diameter})^2 \times (\text{longest diameter}) \times 0.5$. All experimental protocols conducted on the mice were approved by the Tokyo Medical and Dental University Animal Care and Use Committee (A2019-101A).

Immunohistochemistry

Immunohistochemistry was performed as previously described.[14] The resected tumors from the xenograft mouse model were fixed in 10% formaldehyde in PBS for 24 h and stored in 70% ethanol and then embedded in paraffin. The following primary antibodies were

used for immunohistochemistry. The antibody against BRD4 (HPA061646, 1:500) was purchased from Atlas Antibodies (Stockholm, Sweden), and the anti-RPA70 (ab79398, 1:100) antibody was purchased from Abcam. The anti-APEX1 (10203-1-AP, 1:100) antibody was purchased from Proteintech. The anti-POLD4 antibody (MBS9609765, 1:100) was purchased from MyBioSource.com. For measurement of the density per field, each of three images of sections from three tumors treated with *miR-NC* or *miR-1293* were manually captured, and a threshold value was defined for each image using the single point selection tool on the Nikon NIS Elements Br 4.0 software. The sum density was calculated, and the results were normalized to the density values of tumors treated with *miR-NC*.

qRT-PCR

Total RNA was extracted using TRIsure reagent (BIOLINE, London, UK) according to the manufacturer's instructions. For miRNA detection, total RNA was reverse transcribed using the TaqMan Reverse Transcription Kit followed by qRT-PCR performed using Custom TaqMan miRNA assays (Applied Biosystems, Foster City, CA). The miRNA expression level was normalized to that of the internal control *RNU6B*. The following primers were used for the TaqMan assay (Thermo Fisher Scientific): human *miR-1293* (002905) and *RNU6B* (001093).

HR Repair Analysis

The pHPRT-DRGFP vector and the plasmid expressing I-SceI (pCBASce) were gifts from Maria Jasin (Addgene plasmid # 26476; http://www.addgene.org/26476/; RRID: Addgene_26476) (Addgene plasmid # 26477; http://www.addgene.org/26477/; RRID: Addgene_26477).[22,40] U2OS cells were transfected with pHPRT-DRGFP. Puromycin was added 24 h later at 2.5 μg/mL. After puromycin selection, colonies were isolated and analyzed by RT-PCR. U2OS DR-GFP cells contain a single copy of the HR repair reporter substrate DR-GFP, which contains two nonfunctional GFP open reading frames, including one GFP-coding sequence that is separated by a recognition site for the I-SceI endonuclease. The expression of I-SceI leads to the formation of a DSB in the I-SceI GFP allele, which can be repaired by HR using the nearby GFP sequence lacking the N- and C-termini, thereby producing functional GFP that can be detected by flow cytometry. Cells were transfected with *miR-1293* or *miR-NC* for 6–8 h and subsequently transfected with pCBASceI for 48 h. Then, GFP+ cells were analyzed by the Accuri Flow Cytometer.

In Situ Hybridization (ISH) Analysis for the Detection of miRNAs

The ISH assay was performed using miRCURY LNA microRNA ISH Optimization Kit (Exiqon/QIAGEN, Vedbaek, Denmark), as previously described.[41] Briefly, formalin-fixed and paraffin-embedded (FFPE) tissue sections were incubated with proteinase-K (Exiqon/-QIAGEN) for 10 min at 37°C after deparaffinization. Subsequently, the sections were hybridized with digoxigenin (DIG)-labeled *miR-1293* probes (Exiqon/QIAGEN) for 16 h at 60°C and probed with a specific anti-DIG antibody (Sigma) directly conjugated to alkaline phosphatase (AP) (Roche, Basel, Switzerland). Nuclei were counterstained with nuclear fast red (Vector Laboratories, Burlingame, CA).

Public Datasets

To explore the generality of the miRNA expression among colon cancer, ESCC, HNSCC, lung adenocarcinoma, lung squamous cell carcinoma, pancreatic ductal adenocarcinoma, and stomach adenocarcinoma, we examined the public datasets from TCGA (https://cancergenome.nih.gov) retrieved on July 24, 2017. The correlation between prognosis and expression of *miR-1293* in ESCC and HNSCC was analyzed by the Kaplan-Meier Plotter (http://kmplot.com/analysis/), a database that integrates gene expression data and clinical data.[42]

Statistical Analysis

Differences between groups were determined with Student's t test, one-way ANOVA with Bonferroni adjustment, Fisher's exact test, Mann-Whitney U test, or log-rank test as appropriate. All statistical analyses were carried out with R software. p values < 0.05 were considered significant.

SUPPLEMENTAL INFORMATION

Supplemental Information can be found online at https://doi.org/10.1016/j.ymthe.2020.04.001.

AUTHOR CONTRIBUTIONS

Y.T. and Y.G. were involved in the research design, performed the experiments, analyzed the data, and wrote the manuscript. T.M. was involved in the research design, performed the experiments, and analyzed the data. K.T. contributed to public database analysis. J. Inoue was involved in the research design. H.H. supervised the study. J. Inazawa was involved in the research design, wrote the manuscript, and supervised the study.

CONFLICTS OF INTEREST

The authors declare no competing interests.

ACKNOWLEDGMENTS

We thank Ayako Takahashi and Rumi Mori for technical assistance. This work was supported by KAKENHI(18H02688 and 19K07709) from the Ministry of Education, Culture, Sports, Science and Technology (MEXT) and partially supported by the Project for Cancer Research and Therapeutic Evolution (P-CREATE) from Japan Agency for Medical Research and Development, AMED.

REFERENCES

1. Belkina, A.C., and Denis, G.V. (2012). BET domain co-regulators in obesity, inflammation and cancer. Nat. Rev. Cancer *12*, 465–477.

2. Fujisawa, T., and Filippakopoulos, P. (2017). Functions of bromodomain-containing proteins and their roles in homeostasis and cancer. Nat. Rev. Mol. Cell Biol. *18*, 246–262.

3. Zuber, J., Shi, J., Wang, E., Rappaport, A.R., Herrmann, H., Sison, E.A., Magoon, D., Qi, J., Blatt, K., Wunderlich, M., et al. (2011). RNAi screen identifies Brd4 as a therapeutic target in acute myeloid leukaemia. Nature *478*, 524–528.

4. Delmore, J.E., Issa, G.C., Lemieux, M.E., Rahl, P.B., Shi, J., Jacobs, H.M., Kastritis, E., Gilpatrick, T., Paranal, R.M., Qi, J., et al. (2011). BET bromodomain inhibition as a therapeutic strategy to target c-Myc. Cell *146*, 904–917.

5. Shu, S., Lin, C.Y., He, H.H., Witwicki, R.M., Tabassum, D.P., Roberts, J.M., Janiszewska, M., Huh, S.J., Liang, Y., Ryan, J., et al. (2016). Response and resistance to BET bromodomain inhibitors in triple-negative breast cancer. Nature *529*, 413–417.
6. Segura, M.F., Fontanals-Cirera, B., Gaziel-Sovran, A., Guijarro, M.V., Hanniford, D., Zhang, G., González-Gomez, P., Morante, M., Jubierre, L., Zhang, W., et al. (2013). BRD4 sustains melanoma proliferation and represents a new target for epigenetic therapy. Cancer Res. *73*, 6264–6276.
7. Sahai, V., Kumar, K., Knab, L.M., Chow, C.R., Raza, S.S., Bentrem, D.J., Ebine, K., and Munshi, H.G. (2014). BET bromodomain inhibitors block growth of pancreatic cancer cells in three-dimensional collagen. Mol. Cancer Ther. *13*, 1907–1917.
8. Civenni, G., Bosotti, R., Timpanaro, A., Vàzquez, R., Merulla, J., Pandit, S., Rossi, S., Albino, D., Allegrini, S., Mitra, A., et al. (2019). Epigenetic Control of Mitochondrial Fission Enables Self-Renewal of Stem-like Tumor Cells in Human Prostate Cancer. Cell Metab. *30*, 303–318.
9. Donati, B., Lorenzini, E., and Ciarrocchi, A. (2018). BRD4 and Cancer: going beyond transcriptional regulation. Mol. Cancer *17*, 164.
10. Cochran, A.G., Conery, A.R., and Sims, R.J., 3rd (2019). Bromodomains: a new target class for drug development. Nat. Rev. Drug Discov. *18*, 609–628.
11. Stathis, A., and Bertoni, F. (2018). BET proteins as targets for anticancer treatment. Cancer Discov. *8*, 24–36.
12. Lewin, J., Soria, J.C., Stathis, A., Delord, J.P., Peters, S., Awada, A., Aftimos, P.G., Bekradda, M., Rezai, K., Zeng, Z., et al. (2018). Phase Ib trial with birabresib, a small-molecule inhibitor of bromodomain and extraterminal proteins, in patients with selected advanced solid tumors. J. Clin. Oncol. *36*, 3007–3014.
13. Lin, S., and Gregory, R.I. (2015). MicroRNA biogenesis pathways in cancer. Nat. Rev. Cancer *15*, 321–333.
14. Tonouchi, E., Gen, Y., Muramatsu, T., Hiramoto, H., Tanimoto, K., Inoue, J., and Inazawa, J. (2018). miR-3140 suppresses tumor cell growth by targeting BRD4 via its coding sequence and downregulates the BRD4-NUT fusion oncoprotein. Sci. Rep. *8*, 4482.
15. Setten, R.L., Rossi, J.J., and Han, S.P. (2019). The current state and future directions of RNAi-based therapeutics. Nat. Rev. Drug Discov. *18*, 421–446.
16. Anthiya, S., Griveau, A., Loussouarn, C., Baril, P., Garnett, M., Issartel, J.P., and Garcion, E. (2018). MicroRNA-Based Drugs for Brain Tumors. Trends Cancer *4*, 222–238.
17. Vazquez, A., Bond, E.E., Levine, A.J., and Bond, G.L. (2008). The genetics of the p53 pathway, apoptosis and cancer therapy. Nat. Rev. Drug Discov. *7*, 979–987.
18. Yang, F., Zhao, W.J., Jia, C.L., Li, X.K., Wang, Q., Chen, Z.L., and Jiang, Q. (2018). MicroRNA-876-3p functions as a tumor suppressor gene and correlates with cell metastasis in pancreatic adenocarcinoma via targeting JAG2. Am. J. Cancer Res. *8*, 636–649.
19. Fujiwara, N., Inoue, J., Kawano, T., Tanimoto, K., Kozaki, K., and Inazawa, J. (2015). miR-634 activates the mitochondrial apoptosis pathway and enhances chemotherapy-induced cytotoxicity. Cancer Res. *75*, 3890–3901.
20. Sun, C., Yin, J., Fang, Y., Chen, J., Jeong, K.J., Chen, X., Vellano, C.P., Ju, Z., Zhao, W., Zhang, D., et al. (2018). BRD4 Inhibition Is Synthetic Lethal with PARP Inhibitors through the Induction of Homologous Recombination Deficiency. Cancer Cell *33*, 401–416.
21. Stratikopoulos, E.E., Dendy, M., Szabolcs, M., Khaykin, A.J., Lefebvre, C., Zhou, M.M., and Parsons, R. (2015). Kinase and BET Inhibitors Together Clamp Inhibition of PI3K Signaling and Overcome Resistance to Therapy. Cancer Cell *27*, 837–851.
22. Pierce, A.J., Hu, P., Han, M., Ellis, N., and Jasin, M. (2001). Ku DNA end-binding protein modulates homologous repair of double-strand breaks in mammalian cells. Genes Dev. *15*, 3237–3242.
23. Zhou, Y., Dang, J., Chang, K.Y., Yau, E., Aza-Blanc, P., Moscat, J., and Rana, T.M. (2016). MIR-1298 inhibits mutant KRAS-driven tumor growth by repressing FAK and LAMB3. Cancer Res. *76*, 5777–5787.
24. Li, X., Liu, Y., Granberg, K.J., Wang, Q., Moore, L.M., Ji, P., Gumin, J., Sulman, E.P., Calin, G.A., Haapasalo, H., et al. (2015). Two mature products of MIR-491 coordinate to suppress key cancer hallmarks in glioblastoma. Oncogene *34*, 1619–1628.
25. Zhang, Y., Li, M., Ding, Y., Fan, Z., Zhang, J., Zhang, H., Jiang, B., and Zhu, Y. (2017). Serum MicroRNA profile in patients with colon adenomas or cancer. BMC Med. Genomics *10*, 23.
26. Chattopadhyay, E., Singh, R., Ray, A., Roy, R., De Sarkar, N., Paul, R.R., Pal, M., Aich, R., and Roy, B. (2016). Expression deregulation of mir31 and CXCL12 in two types of oral precancers and cancer: importance in progression of precancer and cancer. Sci. Rep. *6*, 32735.
27. Bobola, M.S., Blank, A., Berger, M.S., Stevens, B.A., and Silber, J.R. (2001). Apurinic/apyrimidinic endonuclease activity is elevated in human adult gliomas. Clin. Cancer Res. *7*, 3510–3518.
28. Kelley, M.R., Cheng, L., Foster, R., Tritt, R., Jiang, J., Broshears, J., and Koch, M. (2001). Elevated and altered expression of the multifunctional DNA base excision repair and redox enzyme Ape1/ref-1 in prostate cancer. Clin. Cancer Res. *7*, 824–830.
29. Moore, D.H., Michael, H., Tritt, R., Parsons, S.H., and Kelley, M.R. (2000). Alterations in the expression of the DNA repair/redox enzyme APE/ref-1 in epithelial ovarian cancers. Clin. Cancer Res. *6*, 602–609.
30. Dahai, Y., Sanyuan, S., Hong, L., Di, Z., and Chong, Z. (2013). A relationship between replication protein A and occurrence and prognosis of esophageal carcinoma. Cell Biochem. Biophys. *67*, 175–180.
31. Hoxha, M., Fabris, S., Agnelli, L., Bollati, V., Cutrona, G., Matis, S., Recchia, A.G., Gentile, M., Cortelezzi, A., Morabito, F., et al. (2014). Relevance of telomere/telomerase system impairment in early stage chronic lymphocytic leukemia. Genes Chromosomes Cancer *53*, 612–621.
32. Li, S., Xu, K., Gu, D., He, L., Xie, L., Chen, Z., Fan, Z., Zhu, L., Du, M., Chu, H., et al. (2019). Genetic variants in RPA1 associated with the response to oxaliplatin-based chemotherapy in colorectal cancer. J. Gastroenterol. *54*, 939–949.
33. Zhang, S., Chao, H.H., Wang, X., Zhang, Z., Lee, E.Y.C., and Lee, M.Y.W.T. (2019). Loss of the p12 subunit of DNA polymerase delta leads to a defect in HR and sensitization to PARP inhibitors. DNA Repair (Amst.) *73*, 64–70.
34. Huang, Q.M., Akashi, T., Masuda, Y., Kamiya, K., Takahashi, T., and Suzuki, M. (2010). Roles of POLD4, smallest subunit of DNA polymerase δ, in nuclear structures and genomic stability of human cells. Biochem. Biophys. Res. Commun. *391*, 542–546.
35. Gaillard, H., García-Muse, T., and Aguilera, A. (2015). Replication stress and cancer. Nat. Rev. Cancer *15*, 276–289.
36. Takashima, Y., Kikuchi, E., Kikuchi, J., Suzuki, M., Kikuchi, H., Maeda, M., Shoji, T., Furuta, M., Kinoshita, I., Dosaka-Akita, H., et al. (2019). Bromodomain and extraterminal domain inhibition synergizes with WEE1-inhibitor AZD1775 effect by impairing nonhomologous end joining and enhancing DNA damage in nonsmall cell lung cancer. Int. J. Cancer *1*, 1–12.
37. Stanlie, A., Yousif, A.S., Akiyama, H., Honjo, T., and Begum, N.A. (2014). Chromatin reader Brd4 functions in Ig class switching as a repair complex adaptor of nonhomologous end-joining. Mol. Cell *55*, 97–110.
38. Shimada, Y., Imamura, M., Wagata, T., Yamaguchi, N., and Tobe, T. (1992). Characterization of 21 newly established esophageal cancer cell lines. Cancer *69*, 277–284.
39. Gen, Y., Yasui, K., Kitaichi, T., Iwai, N., Terasaki, K., Dohi, O., Hashimoto, H., Fukui, H., Inada, Y., Fukui, A., et al. (2017). ASPP2 suppresses invasion and TGF-β1-induced epithelial-mesenchymal transition by inhibiting Smad7 degradation mediated by E3 ubiquitin ligase ITCH in gastric cancer. Cancer Lett. *398*, 52–61.
40. Richardson, C., Moynahan, M.E., and Jasin, M. (1998). Double-strand break repair by interchromosomal recombination: suppression of chromosomal translocations. Genes Dev. *12*, 3831–3842.
41. Gokita, K., Inoue, J., Ishihara, H., Kojima, K., and Inazawa, J. (2020). Therapeutic Potential of LNP-Mediated Delivery of miR-634 for Cancer Therapy. Mol. Ther. Nucleic Acids *19*, 330–338.
42. Nagy, Á., Lánczky, A., Menyhárt, O., and Győrffy, B. (2018). Validation of miRNA prognostic power in hepatocellular carcinoma using expression data of independent datasets. Sci. Rep. *8*, 9227.

YMTHE, Volume *28*

Supplemental Information

miR-1293, a Candidate for miRNA-Based Cancer Therapeutics, Simultaneously Targets *BRD4* and the DNA Repair Pathway

Yuki Takagawa, Yasuyuki Gen, Tomoki Muramatsu, Kousuke Tanimoto, Jun Inoue, Hiroyuki Harada, and Johji Inazawa

Figure S1

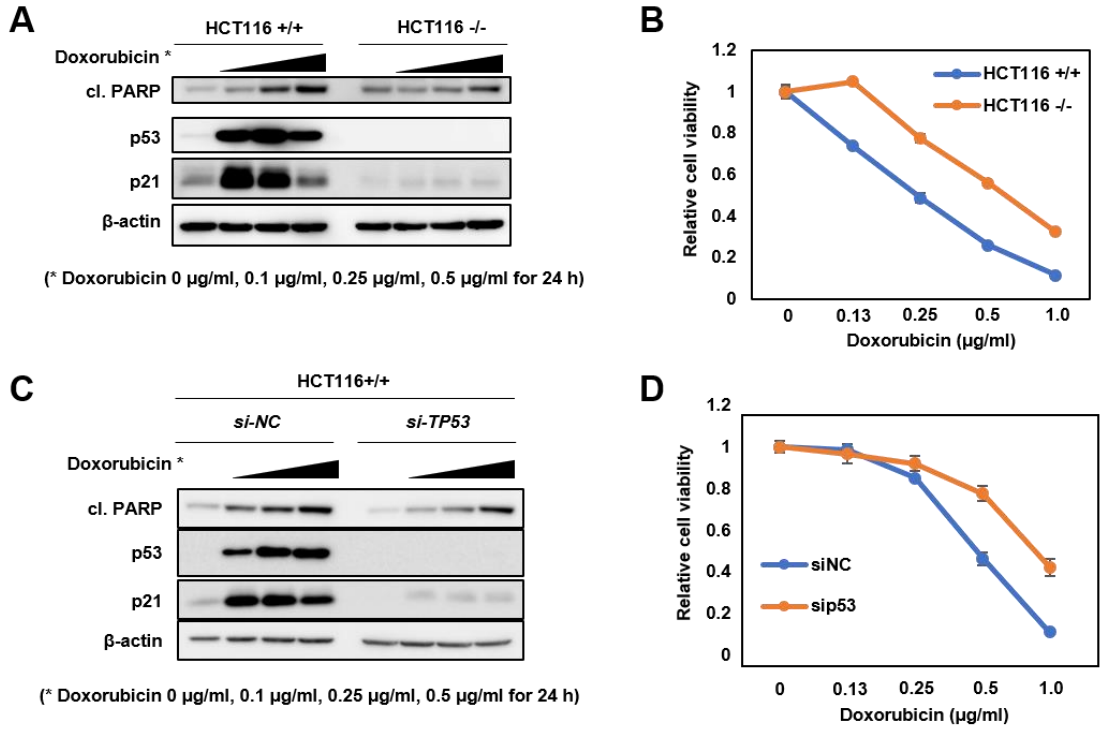

(A) Western blot analysis of cleaved PARP, p53 and p21 in HCT116+/+ and HCT116-/- cells 24 hours after treatment with doxorubicin hydrochloride at the indicated concentrations. **(B)** Dose response curve of doxorubicin at 48 hours after treatment with drug in the HCT116+/+ and HCT116-/- cell lines. The cell growth ratio was assessed by a crystal violet staining assay using a relative ratio compared with DMSO-treated cells. **(C)** Western blot analysis of cleaved PARP, p53 and p21 in HCT116+/+ cells transfected with *si-NC* and *si-TP53* 24 hours after treatment with doxorubicin hydrochloride at the indicated concentrations. **(D)** Dose response curve of doxorubicin at 48 hours after treatment with drug in HCT116+/+ cells transfected with *si-NC* and *si-TP53*. The cell growth ratio was assessed by a crystal violet staining assay using a relative ratio compared with DMSO-treated cells.

Figure S2

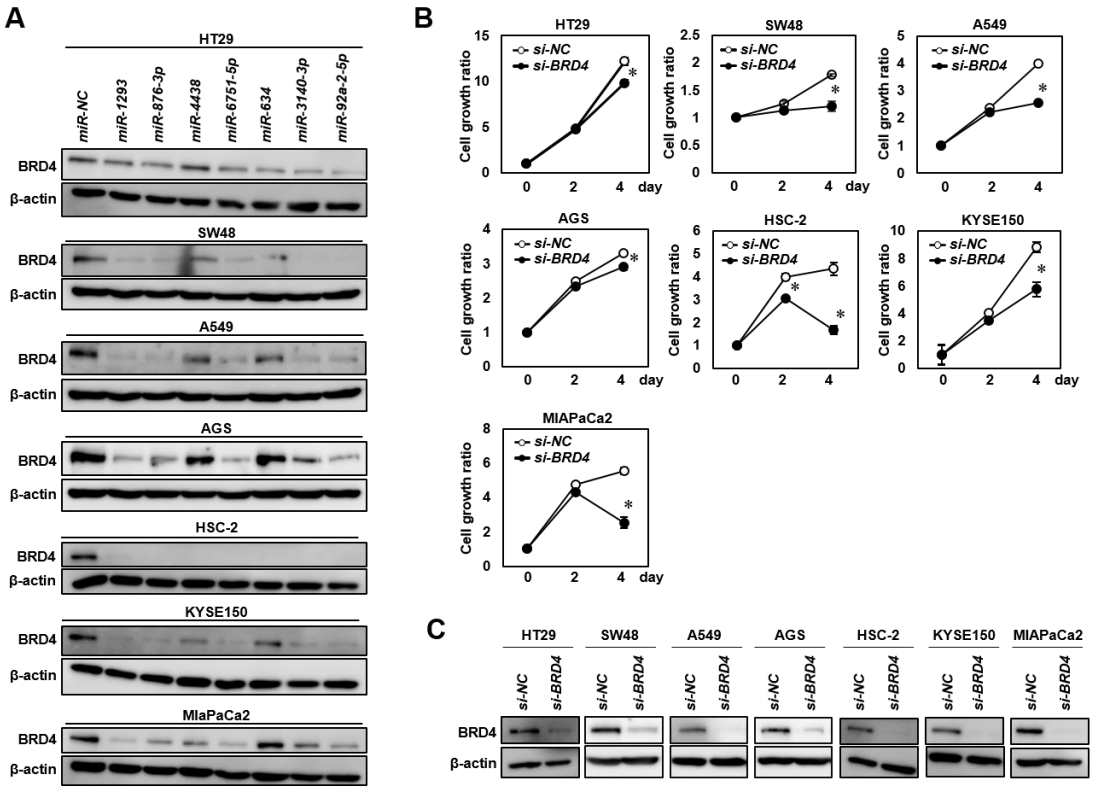

(A) Western blot analysis of BRD4 in HT29, SW48, A549, AGS, HSC-2, KYSE150, and MIAPaCa2 cells 48 hours after transfection with 10 nmol/L *miR-NC* or the indicated 7 miRNAs. **(B, C)** Knocking down *BRD4* suppressed *in vitro* cell proliferation in indicated cells. Cell growth assay (B) and western blot analysis (C) in indicated cells after transfection with 20 nmol/L negative control siRNA (*si-NC*) or siRNA targeting *BRD4* (*si-BRD4*). * $P < 0.05$.

Figure S3

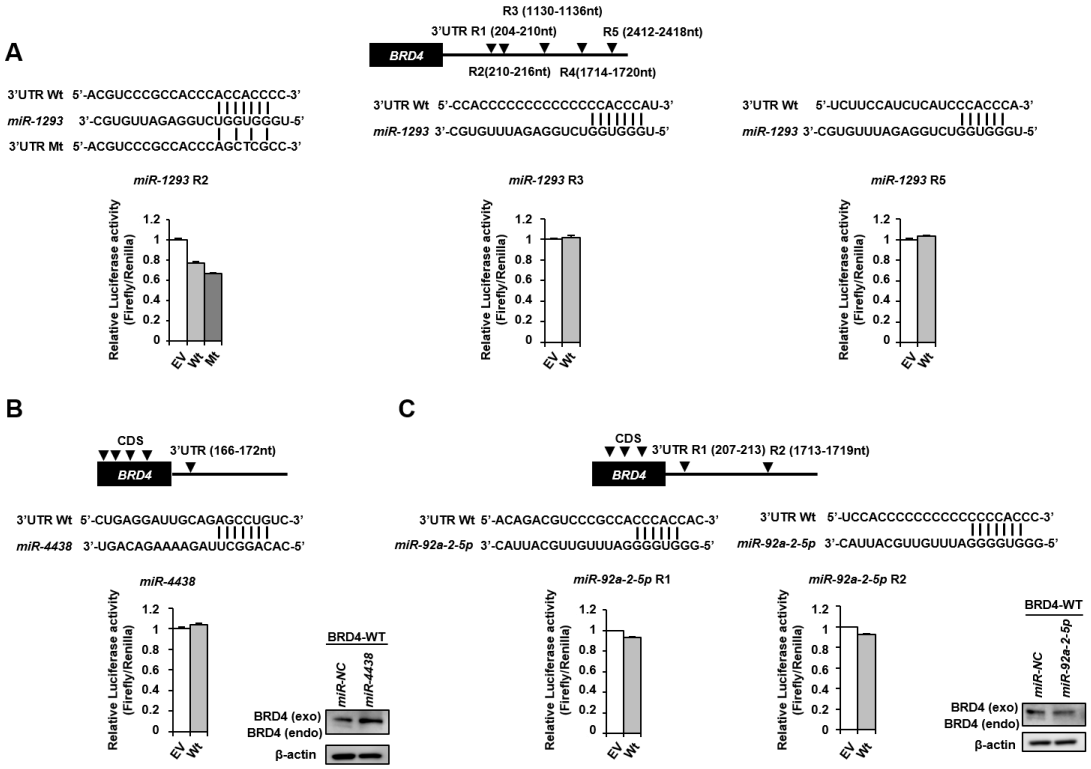

(A-C) Luciferase reporter assay. HOC313 cells were cotransfected with pmirGLO dual-luciferase vectors containing wild-type (WT) *BRD4* or mutant variants of *BRD4* and *miR-NC*, *miR-1293*, *miR-4438* or *miR-92a-2-5p*. Top, putative binding sequence of each miRNA in the 3'UTR or CDS of *BRD4* and mutant sequences are indicated. Bottom, the results of the luciferase assay. Western blot analysis of BRD4 in HOC313 cells. Cells were transfected with the WT BRD4 expression vector, and after 24 hours, 10 nmol/L *miR-NC*, *miR-4438* or *miR-92a-2-5p* was additionally transfected. The expression of exogenous BRD4 was not reduced after transfection with *miR-4438* or *miR-92a-2-5p*.

Figure S4

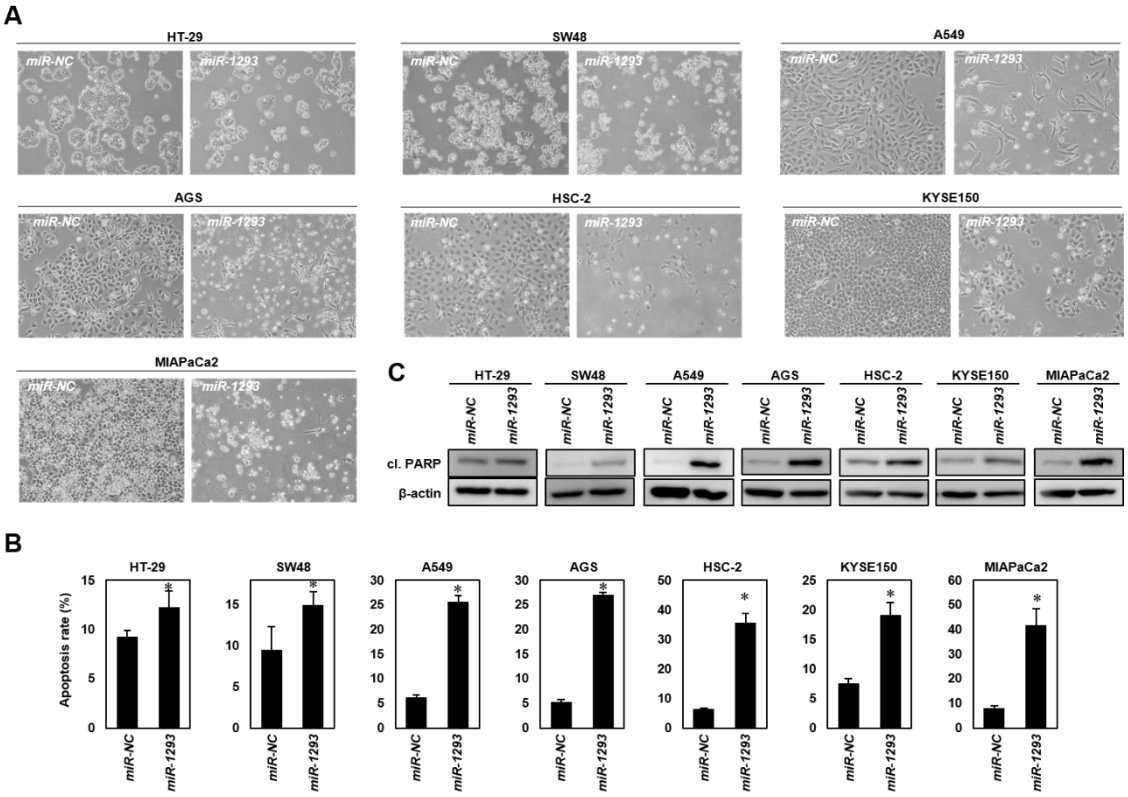

(A) Phase contrast images of indicated cells transfected with 10 nmol/L *miR-NC* or *miR-1293*. Images were obtained 48 hours after transfection. **(B)** The percentage of apoptotic cells in indicated cells transfected with *miR-NC* or *miR-1293*. Cells were double stained with Annexin V and propidium iodide (PI) 48 hours after transfection and analyzed by flow cytometry. The percentage of cells indicates late apoptotic cells (Annexin V+/ PI+). Bar, SD for triplicate experiments. * $P < 0.05$. **(C)** Western blot analysis of cleaved PARP (cl. PARP) in indicated cells 48 hours after transfection with 10 nmol/L *miR-NC* or *miR-1293*.

Figure S5

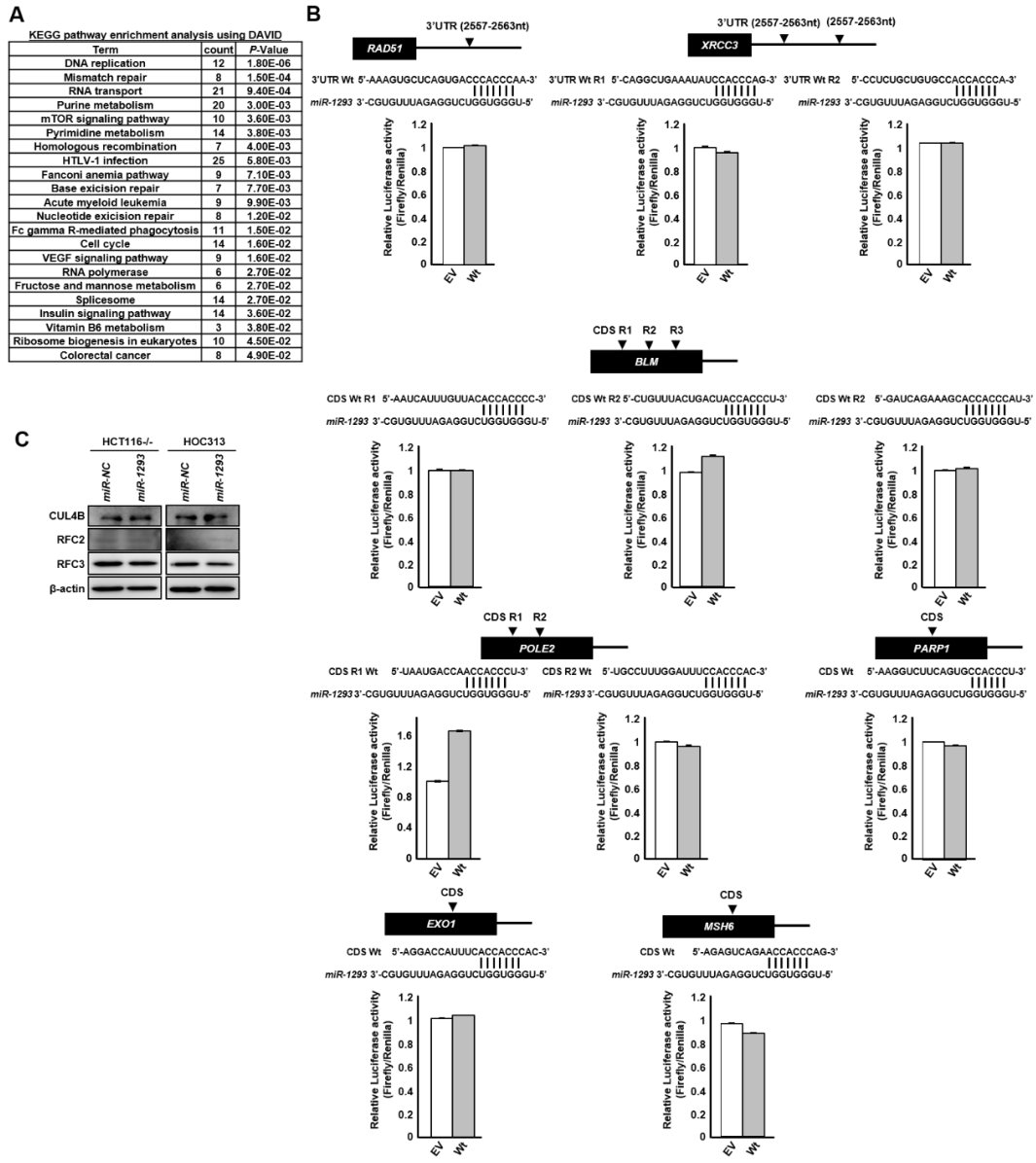

Term	count	*P*-Value
DNA replication	12	1.80E-06
Mismatch repair	8	1.50E-04
RNA transport	21	9.40E-04
Purine metabolism	20	3.00E-03
mTOR signaling pathway	10	3.60E-03
Pyrimidine metabolism	14	3.80E-03
Homologous recombination	7	4.00E-03
HTLV-1 infection	25	5.80E-03
Fanconi anemia pathway	9	7.10E-03
Base excision repair	7	7.70E-03
Acute myeloid leukemia	9	9.90E-03
Nucleotide excision repair	8	1.20E-02
Fc gamma R-mediated phagocytosis	11	1.50E-02
Cell cycle	14	1.60E-02
VEGF signaling pathway	9	1.60E-02
RNA polymerase	6	2.70E-02
Fructose and mannose metabolism	6	2.70E-02
Spliceosome	14	2.70E-02
Insulin signaling pathway	14	3.60E-02
Vitamin B6 metabolism	3	3.80E-02
Ribosome biogenesis in eukaryotes	10	4.50E-02
Colorectal cancer	8	4.90E-02

(A) Table showing the results of the pathway analysis of the 1248 commonly downregulated genes using DAVID Bioinformatics Resources 6.8. Fisher's exact test was used for genes selection. $P < 0.05$ were considered significant. **(B)** Luciferase reporter assays. HOC313 cells cotransfected with pmirGLO dual-luciferase vectors containing the wild-type (WT) 3'UTR or CDS of *RAD51*, *XRCC3*, *BLM*, *POLE2*, *PARP1*, *EXO1* and *MSH6*, and *miR-NC* or *miR-1293*. Top, putative binding site of *miR-1293* within the 3'UTR or CDS of each gene and mutant sequences. Bottom, the results of the luciferase assay. **(C)** Western blot analysis of CUL4B, RFC2 and RFC3 in HCT116-/- and HOC313 cells 48 hours after transfection with 10 nmol/L *miR-NC* or *miR-1293*.

Figure S6

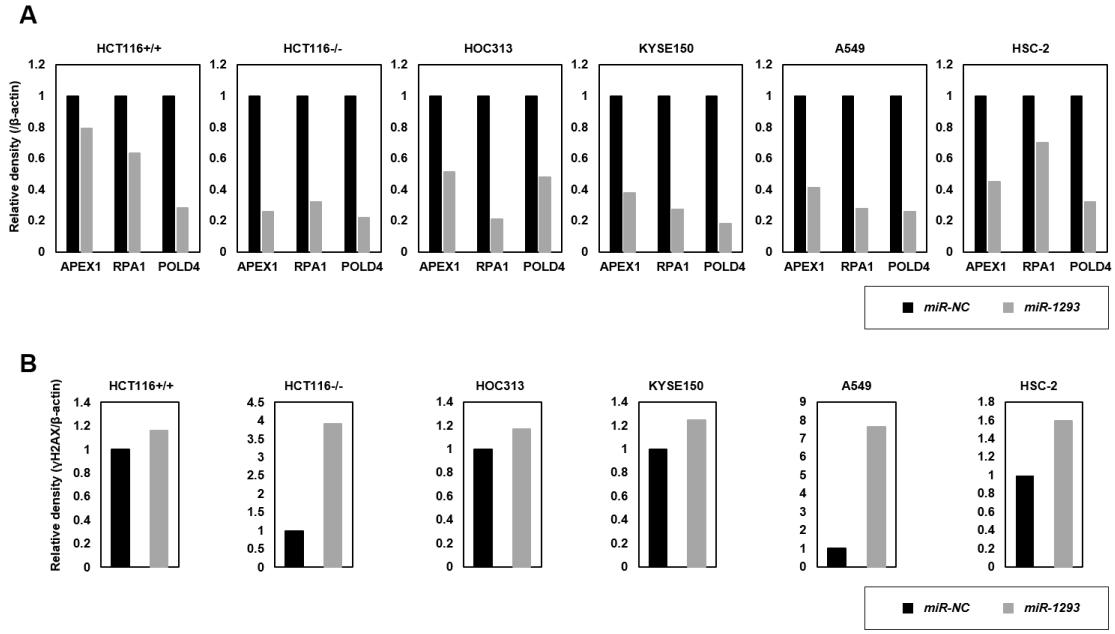

(A, B) Densitometric quantification of the bands in **Figure 4B**. Band intensities of APEX1, RPA1, POLD4 (A), and ɤH2AX (B) were analyzed by Image J software (National Institutes of Health, Bethesda, MA, USA). The values were normalized against β-actin for each sample.

Figure S7

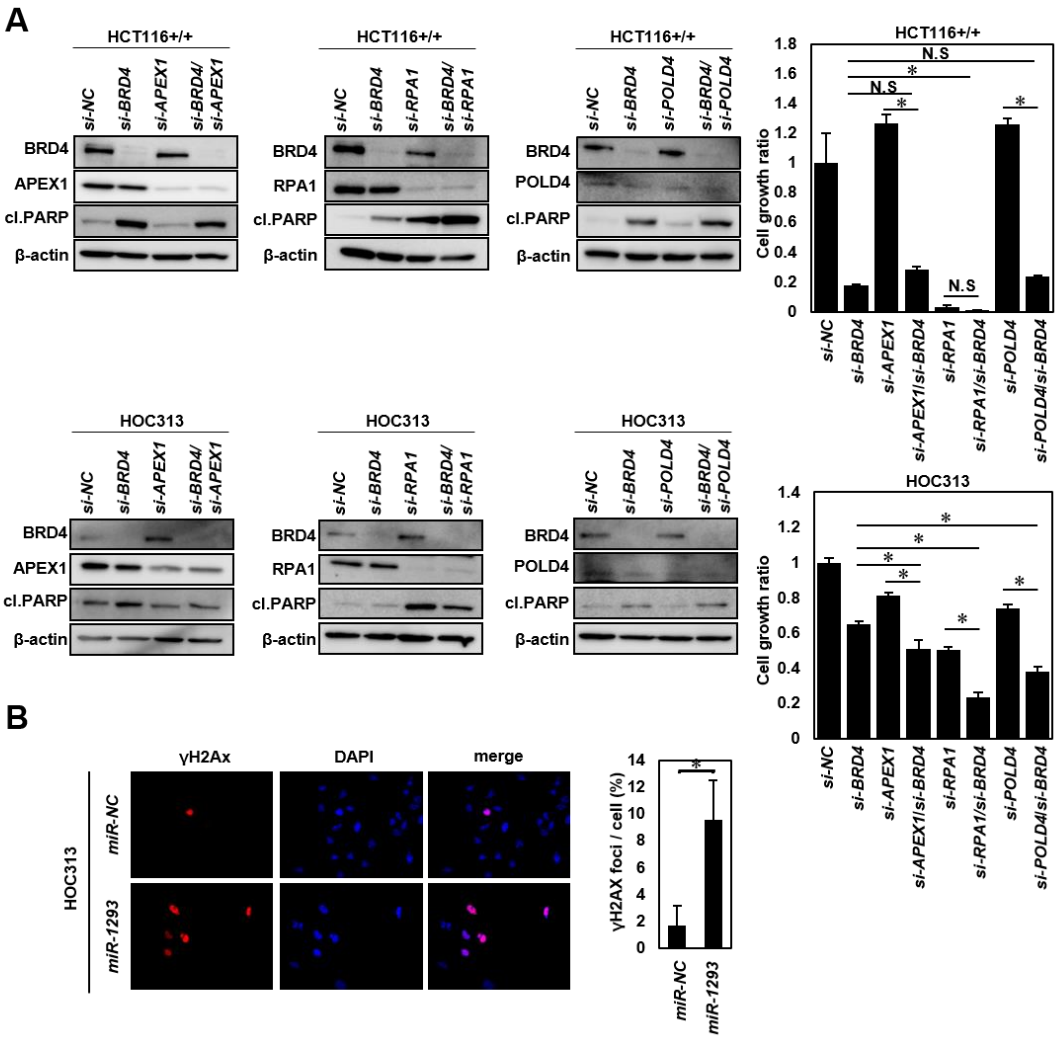

(A) Evaluation of the effect of *si-BRD4* and *si-APEX1*, *si-RPA1* or *si-POLD4* in HCT116+/+ and HOC313 cells. Western blot analysis (left) and cell growth assay (right) in indicated cell lines after transfection with siRNA (*si-NC* (40 nmol/L); *si-BRD4*, *si-APEX1*, *si-RPA1*, and *si-POLD4* (each 20 nmol/L)). After 120 hours of transfection with siRNA, the cell growth rate was assessed with the crystal violet staining assay using a relative ratio compared with the growth of *si-NC*-treated cells. Bar, SD for triplicate experiments. **P* < 0.05. **(B)** Immunofluorescence analysis of HOC313 cells that were double labeled with anti-γH2AX (red) and DAPI (blue; nuclei). Cells were transfected with 10 nmol/L *miR-NC* or *miR-1293* for 6 hours following treatment with neocarzinostatin (200 ng/mL) for 30 minutes.

Figure S8

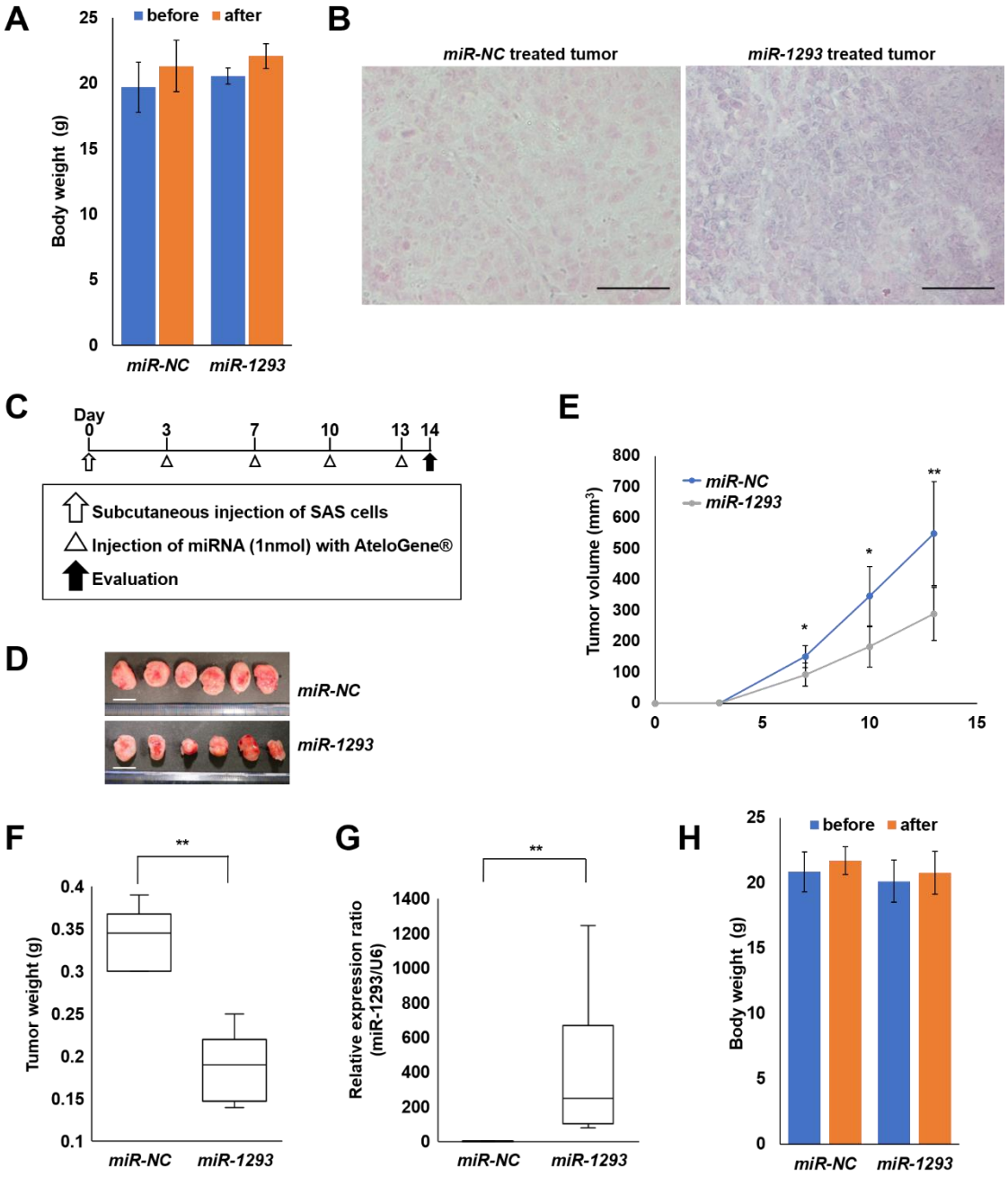

(A) Body weights on day 3 (before the treatment) and on day 19 (after the treatment) were measured. **(B)** Representative images of *in situ* hybridization (ISH) in tumors from mice treated with *miR-NC* or *miR-1293*. The *miR-1293*-specific probe was visualized in purple in the cytoplasm, and the nucleus was counterstained with nuclear fast red. Scale bars, 50 μm. **(C)** The experimental schedule for *miR-1293* treatment in nude mice.

Tumors were formed by subcutaneous injection of SAS cells in nude mice. *miR-NC* or *miR-1293* was administered subcutaneously around the tumors derived from the SAS for a total of 4 times (3, 7, 10 and 13 days after the injection of cells). **(D)** Representative images of tumor-bearing nude mice and resected tumors at 14 days after the injection of HCT116-/- cells. Scale bar, 10 mm. **(E)** Tumor growth curves of xenograft mouse models treated with *miR-NC* or *miR-1293* (n=6, each). Tumor volume was calculated using the following formula: $(\text{shortest diameter})^2 \times (\text{longest diameter}) \times 0.5$. Bar, SD for 6 mice; $*P < 0.05$, $**P < 0.01$. **(F)** Weights of the resected tumors. Tumor weights are shown as a box plot. Bar, SD for 6 mice; $**P < 0.01$. **(G)** Expression analysis of *miR-1293* in the resected tumors. The expression level of *miR-1293* was measured by qRT-PCR. Each experiment was performed in duplicate. The relative ratio was normalized based on the expression of *RNU6B*. Bar, SD for 6 mice; $**P < 0.01$. **(H)** Body weights on day 3 (before the treatment) and on day 14 (after the treatment) were measured.

Figure S9

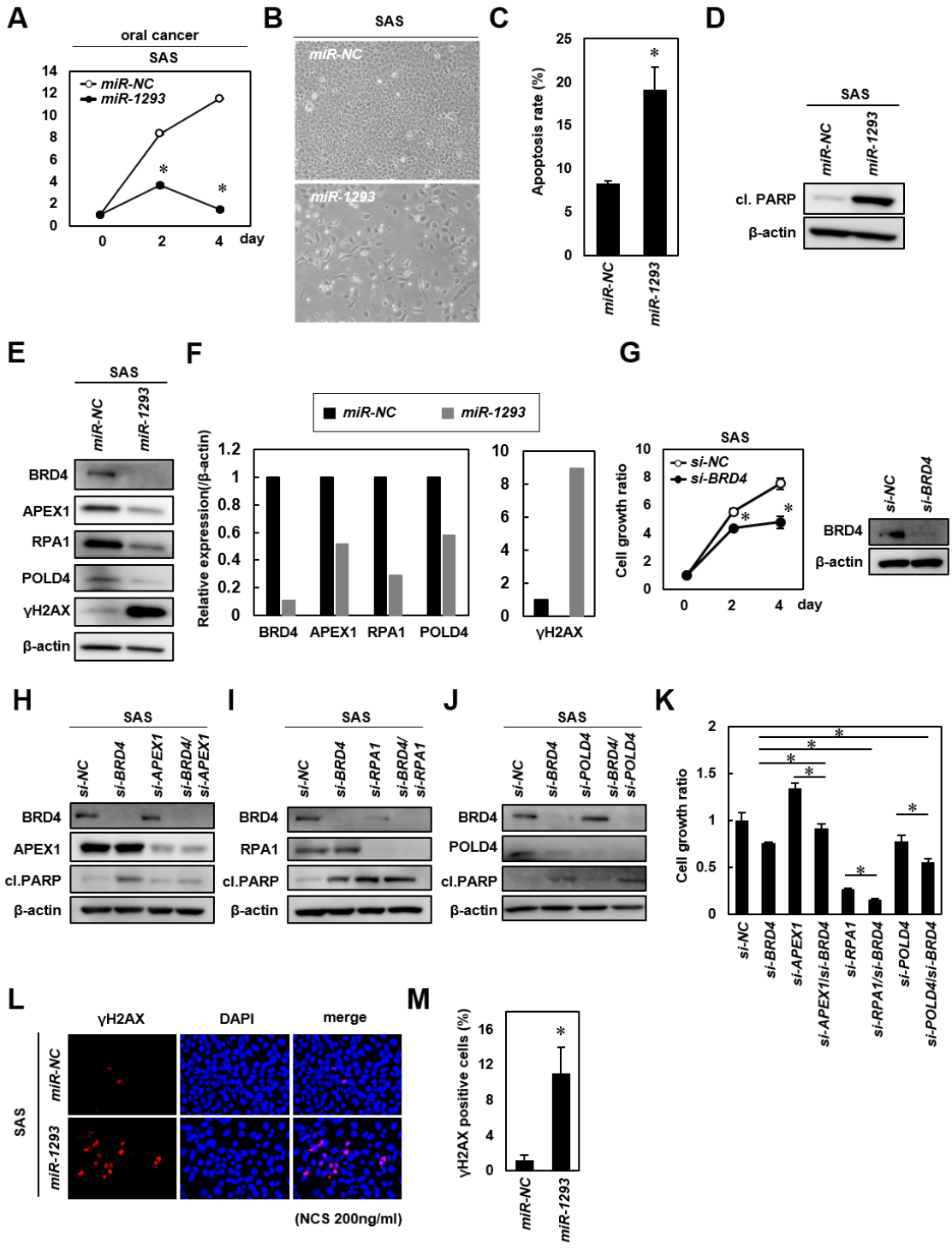

(A) *In vitro* cell growth assay in SAS cells. Cells were transfected with 10 nmol/L *miR-NC* or *miR-1293*. Cell growth rate was assessed with the crystal violet staining assay using a relative ratio compared with cell growth on day 0. Bar, SD for triplicate experiments. *

$P < 0.05$. **(B)** Phase contrast images of SAS cells transfected with 10 nmol/L *miR-NC* or *miR-1293*. Images were obtained 48 hours after transfection. **(C)** The percentage of apoptotic cells in SAS cells transfected with 10 nmol/L *miR-NC* or *miR-1293*. Cells were double stained with Annexin V and propidium iodide (PI) 48 hours after transfection and analyzed by flow cytometry. The percentage of cells indicates late apoptotic cells (Annexin V+/ PI+). Bar, SD for triplicate experiments. * $P < 0.05$. **(D)** Western blot analysis of cleaved PARP (cl. PARP) in SAS cells 48 hours after transfection with 10 nmol/L *miR-NC* or *miR-1293*. **(E)** Western blot analysis of BRD4, APEX1, RPA1, POLD4 and ɣH2AX in SAS cells 48 hours after transfection with 10 nmol/L *miR-NC* or *miR-1293*. **(F)** Western blot band intensities of (E). The band intensities of indicated proteins were analyzed by densitometry and relative protein amounts through normalization against β-actin. **(G)** Knock-down of BRD4 suppressed *in vitro* cell proliferation in SAS cells. Cell growth assay (left) and western blot analysis (right) in SAS cells after transfection with 20 nmol/L negative control siRNA (*si-NC*) or siRNA targeting BRD4 (*si-BRD4*). Bar, SD for triplicate experiments. * $P < 0.05$. **(H-K)** Evaluation of the effect of *si-BRD4* and *si-APEX1*, *si-RPA1* or *si-POLD4*. Western blot analysis (H-J) and cell growth assay (K) in indicated cell lines after transfection with siRNA (*si-NC* (40 nmol/L); *si-BRD4*, *si-APEX1*, *si-RPA1*, and *si-POLD4* (each 20 nmol/L)). One hundred twenty hours following transfection, the cell growth ratio was assessed with the crystal violet staining assay using a relative ratio compared with that of *si-NC*-transfected cells. Bar, SD for triplicate experiments. *$P < 0.05$. knockdown of BRD4 in combination with knockdown of *RPA1*, or *POLD4* led to a more pronounced suppression of *in vitro* cell growth with increased expression of cl. PARP in SAS cells, whereas combination of *si-APEX1* with *si-BRD4* antagonized the growth-suppressive effects of *si-BRD4*. **(L)** Immunofluorescence analysis of SAS cells that were double-labeled with anti-γH2AX (red) and DAPI (blue; nuclei). Cells were transfected with 10 nmol/L *miR-NC*, or *miR-1293* for 6 hours following treatment with neocarzinostatin (200 ng/ml) for 30 minutes. **(M)** The percentage of ɣH2AX-positive cells in (L). *$P < 0.05$.

Figure S10

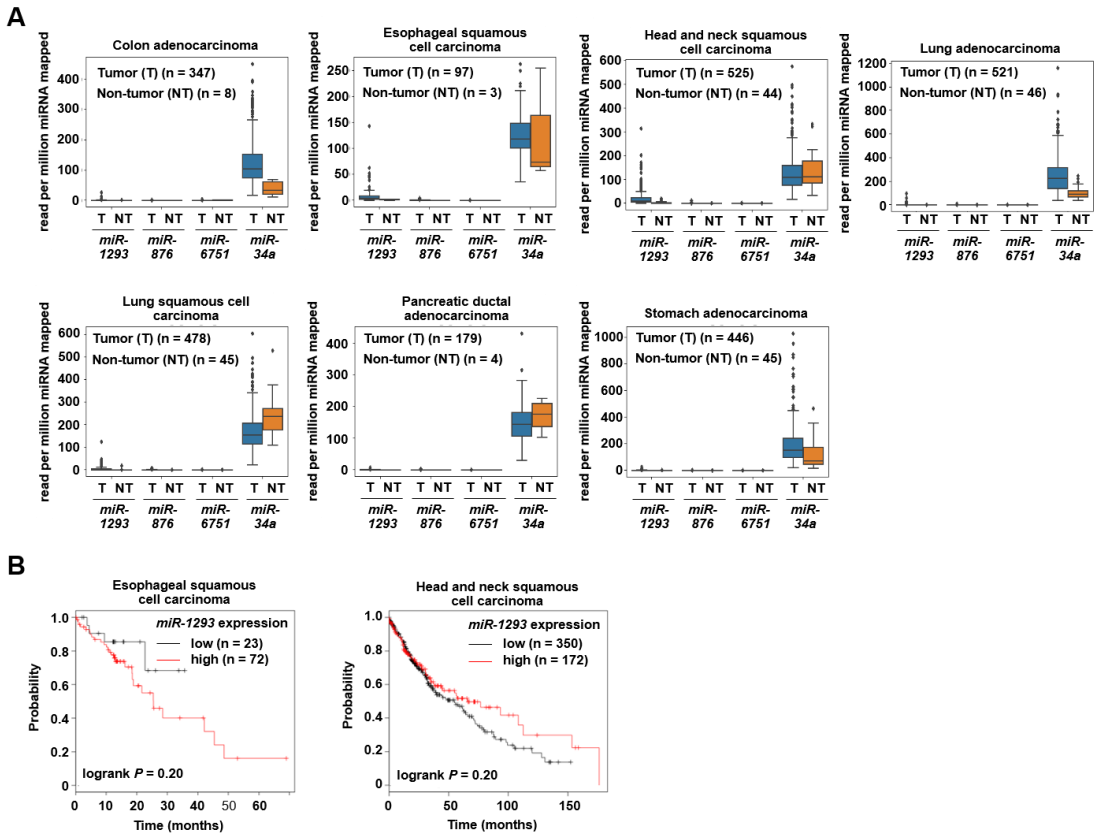

(A) Expression level of *miR-1293*, *miR-876*, and *miR-6751* in primary colon adenocarcinoma, esophageal squamous cell carcinoma (ESCC), head and neck squamous cell carcinoma (HNSCC), lung adenocarcinoma, lung squamous cell carcinoma, pancreatic ductal adenocarcinoma, and stomach adenocarcinoma in TCGA database. In contrast with the expression of *miR-34a*, a representative tumor suppressive miRNA, the expression of *miR-1293*, *miR-876*, and *miR-6751* are extremely low in both tumor tissue (T) and non-tumor tissue (NT), although the expression of *miR-1293* is slightly upregulated in the tumor tissue of ESCC, and HNSCC.

(B) Kaplan-Meier curves for overall survival rates of patients with ESCC and HNSCC According to the Kaplan-Meier Plotter (http://kmplot.com/analysis/). The expression of *miR-1293* is not correlated with overall survival in a corresponding cohort of 95 patients with ESCC, and 522 patients with HNSCC (both $P = 0.20$, log-rank test).